Comparative Study of Stress and Strain Analysis on a Hip End Effector for Orthopedic Surgical Applications Using Different Materials

A Dissertation submitted in partial fulfillment

of the Requirement of the degree of

Master of Engineering

in

Thermal

Engineering

by

Rohan Ganguly

Registration No: 802383005

Under the Supervision of

Dr. Soumya Suddha Mallick

(Professor)

Dr. Ashish Purohit

(Associate Professor)

MECHANICAL ENGINEERING DEPARTMENT
THAPAR INSTITUTE OF ENGINEERING & TECHNOLOGY, PATIALA

August 2025

DECLARATION

I hereby declare that this dissertation is a product of my own work and reflects my original ideas. Where I have incorporated the ideas and words of others, I have duly cited and referenced the original sources. I affirm that I have adhered to the principles of academic honesty and integrity and have not misrepresented, fabricated, or falsified any ideas, data, facts, or sources in this submission. I understand that any breach of the above may result in disciplinary action by the Institute and could also lead to legal consequences if proper citation or permission has not been obtained where required.

Rohan Ganguly

Roll No.: 802383005

Department: Mechanical Engineering

Thapar Institute of Engineering & Technology

Patiala

ABSTRACT

Robotic-assisted total hip arthroplasty (THA) has rapidly advanced as a transformative technology in orthopedic surgery. This innovative approach integrates navigation, minimally invasive techniques, and precise robotic arm control to enhance the accuracy of preoperative planning, implant selection, osteotomy, and artificial joint placement. The inherent accuracy and stability of robotic systems have led to their increasing adoption, particularly in hip and knee arthroplasty, and are recognized for improving implant positioning and reducing limb length discrepancies compared to conventional manual techniques. The precision offered by these systems in achieving planned acetabular positioning and restoring the center of hip rotation is well-documented. While initial clinical outcomes appear largely comparable to traditional methods, the long-term benefits, implant survivorship, time to revision surgery, and cost-effectiveness of robotic THA continue to be areas of active investigation and require further high-quality studies.

A pivotal component underpinning the precision and efficacy of robotic THA is the surgical end effector. This instrument directly engages with bone and tissue during critical surgical phases, such as reaming, cutting, and implant impaction. The structural integrity, mechanical performance, and long-term durability of these end effectors are of paramount importance, directly influencing patient safety and the overall success of the surgical procedure. This thesis undertakes a comprehensive investigation into the stress, strain, and material analysis of a hip end effector specifically designed for orthopedic surgical applications within robotic-assisted platforms.

This study focuses on the mechanical behavior of the hip end effector when fabricated from three distinct and commonly employed biocompatible materials known for their applications in surgical implants and instruments: 17-4 PH stainless steel, Cobalt alloys, and Titanium alloys.

Through detailed computational modeling, specifically employing Finite Element Analysis (FEA), this research aims to meticulously analyze the stress and strain distributions within the end effector design for each chosen material. The analysis will simulate various realistic surgical loading conditions encountered during THA procedures, such as impaction forces, torsional loads, and bending moments, with specific attention to applied loads of **5000 N and 7500 N**. The primary objective is to identify and characterize critical stress concentration points within the end effector structure. This involves determining von Mises stresses, and the corresponding elastic and plastic strains experienced by the device under these loads.

Understanding these critical regions and the magnitudes of stress and strain will provide invaluable insights into the potential areas of mechanical weakness, susceptibility to plastic deformation, and susceptibility to fatigue crack initiation and propagation. This knowledge is crucial for predicting the fatigue life and potential failure modes of the end effector, which in turn will inform material selection, guide structural design optimizations, and enhance the overall reliability and safety of the instrument. The findings from this research are expected to contribute significantly to the ongoing development of more robust, durable, and reliable robotic surgical instruments, thereby playing a vital role in advancing the capabilities and widespread adoption of robotic-assisted arthroplasty, ultimately benefiting patient outcomes.

CERTIFICATE

This is to certify that the dissertation report entitled "**Comparative Study of Stress and Strain Analysis on a Hip End Effector for Orthopedic Surgical Applications Using Different Materials**" submitted by Rohan Ganguly, Registration No. 802383005, in the evaluation of the requirements for the award of the degree of Master of Engineering in Thermal Engineering contains the Bonafide work of his done under our supervision and that the same work has not been submitted elsewhere for the award of any degree to the best of our knowledge.

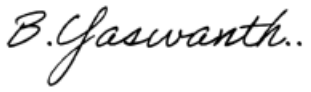

Dr. Soumya Sudha Mallick	Dr. Ashish Purohit	Yaswanth Chandra Bathina
(Professor)	(Associate Professor)	(Quality Engineer)
MED	MED	Stryker Technological
TIET Patiala	TIET Patiala	Center Gurgaon

ACKNOWLEDGEMENT

I would like to sincerely thank all those who have supported and contributed to the successful completion of this thesis. I am deeply grateful to **Dr. Soumya Sudha Mallick** and **Dr. Ashish Purohit** for their academic guidance, valuable insights, and continuous encouragement throughout the course of this work. Their expertise and support have been instrumental in shaping the direction of this research. I would also like to acknowledge **Mr. Nakul Sahani**, my manager, for his understanding and encouragement, which enabled me to manage my professional responsibilities while dedicating time and effort to this thesis. I extend my heartfelt thanks to my guide, **Mr. Yaswanth Chandra Bathina**, for his consistent mentorship, constructive feedback, and unwavering support, which have been critical to navigating the challenges of this research.

My deepest appreciation goes to my friends **Amanpreet Singh**, **Nitesh Kumar**, **Kedar M H**, **Anuj Asati**, and **Vivek Kumar**, whose constant involvement and support played a pivotal role in the progress and completion of this work. Their assistance in technical problem-solving, thoughtful discussions, and data analysis—as well as their emotional support during stressful phases—has been truly invaluable. I am fortunate to have shared this journey with such dedicated and supportive individuals. Finally, I would like to thank everyone who has contributed, directly or indirectly, to the successful realization of this thesis.

TABLE OF CONTENT

LIST OF FIGURES

CHAPTER 1

Motivation

Repeated cracks and fractures observed at the distal end of the hip end effector during the hammering process for reamer handle disassembly raised concerns about its structural reliability. This study is motivated by the need to understand the underlying mechanical behavior that leads to such failures. Using Ansys-based finite element simulations, we aim to accurately model the impact loading conditions, identify high-stress regions, and understand failure mechanisms. Additionally, material analysis will be performed to evaluate the current material's behavior under load, and the maximum force leading to crack initiation will be estimated. These insights will guide improvements in design and material selection, enhancing the reliability and safety of orthopedic instruments in surgical environments.

1. INTRODUCTION

1.1 Background on Orthopedic Tools and Procedures

For patients with traumatic or degenerative musculoskeletal disorders, orthopedic surgery, especially joint replacement procedures, is essential to regaining mobility and enhancing quality of life. It has been demonstrated that total hip arthroplasty (THA), a frequently performed technique, is an excellent treatment for severe hip joint diseases, particularly advanced degenerative and inflammatory illnesses. It has been demonstrated that precise intraoperative cup and stem position and alignment are linked to the clinical results after total hip arthroplasty [26].

With the rising aging population and increasing incidence of osteoarthritis and various other problems such Avascular Necrosis etc. the demand for reliable and efficient hip replacement tools continues to grow.

Successful arthroplasty depends not only on surgical skills but also on the design and performance of specialized **orthopedic tools**. These instruments assist surgeons in accurately preparing bone

surfaces, positioning implants, and securing them within the patient's anatomy. One such critical instrument is the **impactor system**, which is used to seat prosthetic components into place.

The effectiveness of this tool, and more specifically the **hip end effector**, can significantly influence both intraoperative handling and long-term clinical outcomes.

Robotic-Assisted Surgery in Hip Arthroplasty: The Stryker MAKO System

The Stryker MAKO system represents a pivotal advancement in the domain of orthopedic surgery, particularly in procedures such as total hip arthroplasty, total knee arthroplasty, and knee replacement. This robotic-assisted surgical platform integrates image-guided planning with real-time intraoperative support, offering a new paradigm of precision and patient-specific customization that significantly surpasses the capabilities of traditional manual surgical techniques [1].

Figure 1. 1 MAKO Robot (Total Hip Arthroplasty and Total Knee Arthroplasty) [MAKO THA Surgical Guides]

A central innovation of the MAKO system is its utilization of preoperative three-dimensional computed tomography (CT) imaging. This allows for the generation of an anatomically accurate digital model of the patient's joint, facilitating detailed surgical planning tailored to the individual's specific anatomical structure. This personalized planning encompasses critical parameters such as implant size, alignment, and the extent of bone resection required. The use of such preoperative imaging ensures that the surgical strategy is meticulously optimized before entering the operating room, with the goal of enhancing surgical accuracy and improving functional outcomes.

Intraoperatively, the MAKO system assists the surgeon through a robotic arm equipped with haptic feedback technology, specifically the proprietary mechanism. This technology provides multi-modal real-time feedback—tactile, auditory, and visual—that guides the surgeon's hand movements within the pre-defined boundaries established during the planning phase. The system is designed to halt or restrict the movement of the surgical tool if it deviates from these boundaries, thereby protecting essential anatomical structures such as ligaments, nerves, and healthy bone tissue. Although the robotic arm provides this enhanced level of control and precision, it is important to note that the system is not autonomous; the surgeon maintains full operational authority throughout the procedure.

The collaborative nature of the MAKO system—merging robotic precision with human clinical expertise—has been associated with a range of clinical benefits. These include improved implant alignment, reduced intraoperative variability, and potentially shorter recovery times. Studies and clinical experience suggest that the system contributes to more consistent surgical outcomes, lower postoperative pain levels, and increased patient satisfaction compared to conventional surgical techniques. Furthermore, the reduction in intraoperative complications and the improved preservation of soft tissues may also contribute to shorter hospital stays and faster rehabilitation.

In a broader context, the MAKO system is indicative of a wider technological evolution within surgical practice, reflecting a shift toward minimally invasive, data-driven, and precision-focused interventions. As robotic surgical platforms become increasingly sophisticated, their integration into routine clinical practice is expected to grow, not as a replacement for the surgeon, but as a tool that enhances surgical performance and patient care.

In summary, the Stryker MAKO robotic system exemplifies the future direction of orthopedic surgery. Its combination of advanced imaging, real-time feedback, and precise intraoperative control offers substantial improvements in surgical safety, accuracy, and outcomes. The MAKO system thus stands as a model of how robotic technologies can successfully augment human capabilities in the operating room, setting a new standard for excellence in orthopedic care [18].

The hip joint plays a vital role in human mobility and bears substantial loads during daily activities such as walking, running, and climbing. In orthopedic surgeries, particularly hip replacement procedures, specialized surgical instruments such as the hip end effector are used for tasks like reaming, positioning, and alignment. One critical issue observed in surgical practice is the occurrence of cracks and fractures at the distal end of the hip end effector during the hammering process used to disassemble the reamer handle. Such mechanical failures raise concerns about structural integrity and long-term reliability [18].

1.2 Importance of the Hip End Effector in Arthroplasty

The hip end effector plays a pivotal role in total hip arthroplasty (THA), a surgical procedure aimed at replacing damaged or diseased hip joints to restore mobility and reduce pain. As a critical component of the surgical instrumentation, the hip end effector directly interacts with the patient's anatomy, enabling precise manipulation, positioning, and stabilization of implants during the operation. Its design and functionality significantly influence surgical accuracy, operative time, and patient outcomes [1].

For surgical procedures to be performed correctly, end effector dexterity is essential. The job of manipulating equipment and tissues falls to end-effectors. They can reach and grasp sometimes very sensitive tissues because of their small size and incredibly sharp tip. Titanium and stainless steel, which are impervious to corrosion and deterioration, can be used to construct reusable end effectors [18].

One of the primary functions of the hip end effector is to securely hold and guide the reaming tools that prepare the acetabulum (hip socket) for implant placement. Accurate reaming ensures optimal fit and alignment of the prosthetic components, which are essential for the longevity and

biomechanical performance of the implant. Additionally, the end effector must accommodate varying anatomical shapes and sizes, requiring adaptability and reliable gripping mechanisms.

Furthermore, the hip end effector must withstand high mechanical loads and repetitive stress throughout the surgical procedure while maintaining ergonomic ease for the surgeon. Advances in material selection and design optimization have enhanced the durability, precision, and safety of these devices. Overall, the hip end effector is indispensable for ensuring surgical precision, minimizing complications, and improving the success rates of hip arthroplasty surgeries.

1.3 Problem Definition

In the field of orthopedic biomechanics, the design and material selection of hip end effectors play a crucial role in ensuring implant durability, patient safety, and long-term performance. These components are subjected to complex loading conditions, including high-impact and cyclic loads, which demand materials with excellent mechanical strength, fatigue resistance, and biocompatibility. However, the choice of optimal material remains a challenge due to varying mechanical properties, manufacturing constraints, and biological considerations. Among the most used materials in medical implants are 17-4 PH stainless steel, titanium alloys, and cobalt-based alloys—each offering distinct advantages and limitations in terms of stress handling, deformation behavior, and compatibility with the human body. A comparative analysis of these materials under realistic loading scenarios is essential to identify the most suitable material for hip end effector applications. This study aims to fill this gap by performing a detailed stress-strain analysis using finite element methods to evaluate and compare the mechanical response of these three materials under standardized loading conditions.

1.4 Objectives of the Study

his study aims to investigate and compare the mechanical performance of three widely used biomedical materials—17-4 PH stainless steel, titanium alloy, and cobalt alloy—specifically for their application in hip end effectors. These materials are commonly selected in orthopedic applications due to their high strength, corrosion resistance, and biocompatibility. However, their

behavior under stress and strain conditions can vary significantly, which directly impacts the performance, durability, and safety of the end effector during use.

To address this, the study sets out to achieve the following objectives:

- **To evaluate** the stress and strain responses of each material under a standardized load using Finite Element Analysis (FEA).
- **To analyze and compare** the deformation characteristics, stress distribution, and strain concentrations across the three materials.
- **To identify** the most suitable material for hip end effector applications based on mechanical performance criteria such as strength, stiffness, and resistance to deformation.
- **To provide** a data-driven basis for material selection in biomedical device design, thereby enhancing the reliability and efficiency of orthopedic tools.

By fulfilling these objectives, the study seeks to support more informed decision-making in the design and material selection of hip end effectors used in clinical practice.

1.5 Scope and Limitations of the Study

The present study is focused on the **material selection and structural analysis** of the hip end effector used in orthopedic surgeries, specifically in total hip arthroplasty. The work includes computational modeling, material selection, and simulation-based evaluation.

The following are the key **boundaries** and **limitations** of this research:

- The study considers only the **mechanical aspects** of the design; it does not include biological interactions, such as tissue response or long-term biocompatibility.
- The analysis is limited to **static simulations** using finite element methods.
- Tool manufacturing processes, sterilization considerations, and economic aspects are beyond the scope of this thesis.
- The study does not cover integration with robotic surgical systems or feedback-based control systems.

Despite these limitations, the research offers a detailed mechanical insight into stress-related failure points and proposes a validated alternative that aligns with surgical requirements.

1.6 Need for the Study

Given the growing global demand for joint replacement surgeries and the increasing complexity of modern orthopedic procedures, the need for robust, durable, and high-performance surgical tools—such as hip end effectors—is more critical than ever. These components must endure substantial mechanical loads, including high-impact forces and cyclic stresses, particularly during robotic-assisted and minimally invasive surgeries. Despite the widespread use of materials like titanium alloy, 17-4 PH stainless steel and cobalt alloy in biomedical applications, there remains a lack of comparative research focused on their stress-strain behavior under identical loading conditions relevant to hip end effectors. Failures arising from high stress concentrations can compromise surgical precision, reduce tool lifespan, and pose risks to patient safety.

This study addresses this critical gap by evaluating and comparing the mechanical performance of these materials through finite element analysis, with the aim of identifying the most suitable candidate for improved structural reliability. The findings are especially timely and relevant for advancing the design of orthopedic instruments that prioritize precision, compactness, and longevity.

CHAPTER 2

LITERATURE REVIEW

2.1 Review of Hip Arthroplasty Tools and Devices

Hip arthroplasty has evolved significantly over the decades, with continuous advancements in surgical techniques and instrumentation aimed at improving clinical outcomes and procedural efficiency. Hip arthroplasty tools and devices have revolutionized hip replacement surgery, transforming it into a highly precise and almost futuristic procedure that combines cutting-edge technology with surgical expertise. Traditional tools used in total hip replacement procedures include reamers, broaches, impactors, and alignment guides, each serving a specific role in bone preparation and implant placement.

Modern developments have led to the design of more ergonomic and precise instruments that reduce intraoperative time and enhance implant alignment. Surgeons now utilize **robot-assisted systems** that provide unparalleled stability and accuracy, allowing for perfectly guided bone cuts and implant positioning. These systems integrate with **computer navigation technology**, which creates a detailed 3D map of the patient's hip in real time, enabling surgeons to customize every step of the operation to the patient's unique anatomy. Instruments equipped with **smart sensors** measure force, angle, and pressure, delivering constant feedback that helps avoid errors and ensures optimal implant alignment—critical factors that dramatically improve joint function and longevity. On the device side, implants have evolved from simple metal and plastic parts to **high-tech 3D-printed titanium alloys with porous surfaces that encourage natural bone growth**, along with advanced ceramics that resist wear and reduce inflammation. Some implants even feature **bioactive coatings** that promote faster healing and reduce the risk of infection. Additionally, modular implant designs allow surgeons to mix and match components during surgery for the perfect fit and function. These innovations collectively reduce surgery time, minimize complications, and extend implant lifespan, often giving patients a new hip that feels and moves like their original joint. This incredible fusion of robotics, smart tools, and bioengineered implants marks a monumental leap forward, turning hip arthroplasty from a

challenging operation into a near-perfect science—offering patients pain relief, restored mobility, and a dramatically improved quality of life.

Notably, the integration of modular components and minimally invasive tool designs has improved surgical access and reduced patient trauma. However, despite these improvements, several studies have highlighted persistent challenges related to tool durability, particularly under repeated mechanical stress. End effectors, which interface directly with implants during hammering or impaction, are often subjected to high axial loads, leading to material fatigue, micro-cracks, or in some cases, complete failure. These issues underscore the importance of material selection, geometry optimization, and stress distribution analysis in the design of arthroplasty tools. The literature emphasizes the need for robust design methodologies and finite element-based evaluations to mitigate such failures and ensure consistent surgical performance.

The field of robotic-assisted arthroplasty, particularly in total hip arthroplasty (THA) and total knee arthroplasty (TKA), has seen rapid advancements aimed at improving precision and patient outcomes. This literature review synthesizes key findings from recent studies exploring the efficacy, safety, and operational considerations of robotic assistance compared to conventional manual techniques.

Early reviews highlighted the transformative potential of robotic arm-assisted arthroplasty. Their work underscored its capabilities in enabling accurate preoperative planning, optimal selection of implants, minimally invasive surgical approaches, precise osteotomy, and accurate artificial joint placement. These attributes, stemming from technology's inherent accuracy and stability, position robotic systems as a rapidly developing area within joint surgery [1].

However, the question of whether this enhanced precision translates to superior clinical outcomes remains a central point of investigation. A systematic review and meta-analysis specifically examined robot-assisted THA versus conventional manual techniques. While they affirmed that robotic assistance indeed improves implant positioning accuracy, their findings suggested limited data to conclude that this improved accuracy leads to better long-term clinical outcomes. Furthermore, they did not identify significant differences in complication rates or implant survivorship, noting a tendency for prolonged surgical times with robotic procedures [10]. Supporting this, a systematic review and meta-analysis also found that while robotic assistance

improved cup positioning accuracy and reduced outliers, it did not significantly alter clinical outcomes or leg length discrepancy, and often increased operation time [7].

These findings about the current use of robotics in total hip arthroplasty are further supported by the increased precision of acetabular cup positioning and hip rotation center restoration made possible by robotic devices. Importantly, when compared to manual techniques, these accuracy gains had not yet resulted in differences in early functional outcomes, correction of leg-length discrepancies, or postoperative complications.

In contrast, practical limitations included high installation costs, additional radiation exposure, steep learning curves for surgeons, and compatibility issues with restricted implant designs [8]. mirrored these opinions, stating that while robotic THA improved radiological results, functional results were "equivocal". Additionally, the cost of robotic total hip arthroplasty and the already remarkable outcomes of traditional procedures have hindered its global appeal [3]. The thorough review of meta-analyses reaffirmed the general agreement that robot-assisted THA enhances radiography results. There is still a persisting knowledge gap, nevertheless, as its effects on complication rates, clinical and functional outcomes, and implant survival are still unknown [9].

In addition to THA, other arthroplasty procedures are also being investigated with robotic help. For simple unilateral knee osteoarthritis, a single-center retrospective study comparing MAKO robot-assisted total knee arthroplasty (TKA) with traditional manual TKA, with an emphasis on safety and effectiveness in the early postoperative phase. This implies continued research into uses and preliminary results [13]. The scoping review on robotic-assisted hip and knee revision arthroplasty indicated growing areas of research by highlighting the wider scope of robotic uses in orthopedic surgery, including revisions [15].
More cup anteversion and a larger percentage of components within safe ranges were identified in the meta-analysis on MAKO robot-assisted THA, with forgotten joint scores favoring MAKO [13]. Recent research are further refining our understanding of the benefits of robotics. Similarly, using MAKO robotic assistance, improved radiographic characteristics and higher postoperative rates were observed with a focus on hip osteoarthritis. These results point to minor clinical benefits and ongoing radiography accuracy with particular robotic systems [14].

The importance of precise implant positioning tailored to individual patient biomechanics, especially considering spinopelvic mobility had proposed that robotic-arm assisted THA facilitates enhanced planning based on patient-specific factors, enabling more accurate functional component positioning [8]. This area was further reviewed and discussed robotic-assisted THA in the context of spinopelvic parameters, emphasizing the dynamic relationship between the pelvis and lumbar spine as a critical factor in hip stability [16].

From an operational perspective practical procedure guide for robotic arm-assisted (MAKO) THA, outlining pre-operative was provided on preparation, surgical steps, and precautions, indicating the growing adoption and need for standardized procedures for these advanced techniques [14]. Additionally, economic benefits, specifically noting a reduction in implant waste associated with robotic-assisted THA, suggesting potential cost efficiencies in the long run [5]. Finally, a broader review of surgical robotics was provided, discussing current platforms and the crucial role of end effectors, indicating the continuous innovation in this technological domain driven by expiring patents and evolving surgical needs [18].

In conclusion, the literature largely agrees that robotic assistance significantly enhances the accuracy and precision of implant placement in arthroplasty. While the translation of this radiographic superiority into consistently improved long-term functional and clinical outcomes remains an area requiring further high-quality research, ongoing studies suggest benefits in specific patient-reported outcomes and operational efficiencies. The continued evolution of robotic platforms and surgical techniques, alongside a deeper understanding of patient-specific biomechanics, points towards a growing, albeit still maturing, role for robotics in joint arthroplasty.

2.2 Summary of Research Gaps

1. **Chen, Deng, Sun, and He (2022)** conducted a review highlighting robotic arm-assisted arthroplasty's latest developments, emphasizing its role in achieving accurate preoperative planning, optimal implant selection, minimally invasive surgery, precise osteotomy, and accurate artificial joint placement due to its high accuracy and stability.
2. **Kumar, Patel, Baburaj, Rajnish, and Aggarwal (2023)** performed a systematic review and meta-analysis comparing robot-assisted total hip arthroplasty (THA) to conventional manual techniques. They concluded that while robotic assistance improves implant positioning accuracy, there is currently limited data to suggest this translates to better long-

term clinical outcomes, and they found no significant differences in complication rates or implant survivorship. They also noted prolonged surgical times for robotic procedures.

3. **Kayani, Konan, Ayuob, Ayyad, and Haddad (2019)** reviewed the current role of robotics in THA. Their findings indicated that robotic THA improves accuracy in achieving planned acetabular cup positioning and precision for restoring the hip's center of rotation. However, this enhanced accuracy did not result in differences in early functional outcomes, correction of leg-length discrepancy, or postoperative complications compared to conventional manual THA. They also identified limitations such as high installation costs, additional radiation exposure, and steep learning curves.
4. **Bullock, Brown, Clark, Plant, and Blakeney (2023)** provided a current concepts article on robotics in THA. They reported that while robotic THA consistently shows improved radiological outcomes (implant placement accuracy), the evidence regarding functional outcomes remains equivocal when compared to conventional techniques. They also highlighted the limited literature on newer robotic systems beyond MAKO and ROBODOC, alongside challenges related to cost and the already high success rates of traditional methods.
5. **Han, Chen, Zhang, Han, Wei, Li, and Wei (2019)** conducted a systematic review in addition of meta-analysis comparing robotics-assisted versus conventional manual approaches for THA. They concluded that robotic assistance significantly improves the accuracy of cup positioning and reduces outliers but did not find significant differences in clinical outcomes (e.g., WOMAC scores, complications) or leg length discrepancy. They also noted an increase in operation time for robotic procedures.
6. **Cepolina and Razzoli (2024)** reviewed robotic surgery platforms and end effectors, discussing the extensive growth of automated surgical devices. They noted that expiring patents are broadening the common knowledge base for future surgical robotics development. Their review covered the advantages and limitations of various robotic systems, with a particular focus on the crucial role of end effectors in surgical outcomes.
7. **Kort, Stirling, Pilot, and Müller (2021)** conducted a systematic overview of meta-analyses comparing robot-assisted THA to conventional THA. They concluded that robot-assisted THA improves radiographic outcomes (implant positioning accuracy), but it

remains unclear whether it alters complication rates, clinical and functional outcomes, and implant survival.

8. **Ma, Sun, Xin, Zhong, Xie, and Xiao (2024)** performed a single-center retrospective analysis comparing the efficacy and safety of MAKO robot-assisted total knee arthroplasty (MA-TKA) with conventional manual total knee arthroplasty (CM-TKA) in patients with end-stage knee osteoarthritis during the early postoperative period.
9. **Fontalis, Raj, Kim, Gabr, Glod, Foissey, Kayani, Putzeys, and Haddad (2023)** presented a manuscript outlining challenges posed by spinopelvic imbalance and a reproducible approach to achieve functional-component positioning in THA. They concluded that robotic-arm assisted THA has facilitated enhanced planning based on patient-specific biomechanics and spinopelvic mobility, enabling precise functional component positioning.
10. **Cheng, Chiu, McLawhorn, Westrich, Green, and Cross (2024)** investigated the reduction in implant waste associated with robotic-assisted total hip arthroplasty.
11. **Llombart-Blanco, Mariscal, Barrios, Vera, and Llombart-Ais (2024)** conducted a comprehensive meta-analysis comparing the efficacy and safety outcomes of MAKO robot-assisted total hip arthroplasty. They found that the MAKO group achieved greater cup anteversion and a higher percentage of components within safe inclination and anteversion ranges. While Harris Hip Scores did not differ significantly, forgotten joint scores favored MAKO, though not exceeding the minimally clinically significant difference.
12. **Loke, Lim, Chan, and Tan (2025)** performed a systematic review in addition of meta-analysis comparing MAKO robotic-arm-assisted THAs (MAKO-THA) to conventional methods for hip osteoarthritis. Their findings indicated that MAKO-assisted THAs resulted in higher postoperative Harris Hip Scores (HHS) and improved radiographic parameters (implant positioning accuracy).

CHAPTER 3

SYSTEM DESCRIPTION AND FUNCTIONAL ANALYSIS

3.1 Introduction

The integration of robotic systems in orthopedic surgery has revolutionized the field, particularly in total hip arthroplasty (THA). A critical component of these robotic systems is the hip end effector, which serves as the mechanical interface between the robotic arm and the surgical instruments. This chapter provides a detailed description of the hip end effector, its functionality during surgical operations such as reaming, broaching, and impaction, and an explanation of impaction and load transmission. The chapter concludes with schematic diagrams illustrating the system's design and operation.

3.2 Detailed Description of the Hip End Effector

The hip end effector is designed to accurately transmit robotic arm's movements to the surgical instruments while maintaining the necessary alignment and force application. Constructed from high-strength, biocompatible materials such as titanium alloys, the end effector ensures durability and resistance to corrosion. The design incorporates modular interfaces that allow for the attachment of various surgical tools, including reamers, broaches, and implant inserters.

Figure 3. 1- Structural and Functional Components of a Hip End Effector with Offset Reamer Handle

Key features of the hip end effector include:

- **Modular Tool Interface**: Allows for quick attachment and detachment of surgical instruments, facilitating efficient transitions between different surgical tasks.
- **Force and Torque Sensors**: Embedded sensors provide real-time feedback on the forces and torques applied during surgery, enabling the robotic system to adjust movements accordingly.
- **Ergonomic Design**: The effector's design minimizes the risk of strain and fatigue for the surgical team, enhancing overall efficiency and safety.

3.3 Functionality During Surgical Operations

Figure 3. 2-Fully Assembled Reamer and Power Equipment in MAKO [18]

3.3.1 Reaming

Reaming is the process of enlarging the acetabular cavity to accommodate the acetabular component of the hip implant. During this phase, the hip end effector guides the reamer into the acetabulum, ensuring precise alignment and depth. The embedded force sensors monitor the resistance encountered, allowing the robotic system to adjust the reaming speed and pressure to prevent over-reaming or damage to surrounding bone structures.

Figure 3. 3- Initial reaming with the tip of the reamer constrained and the trajectory unconstrained

[MAKO THA Surgical Guides]

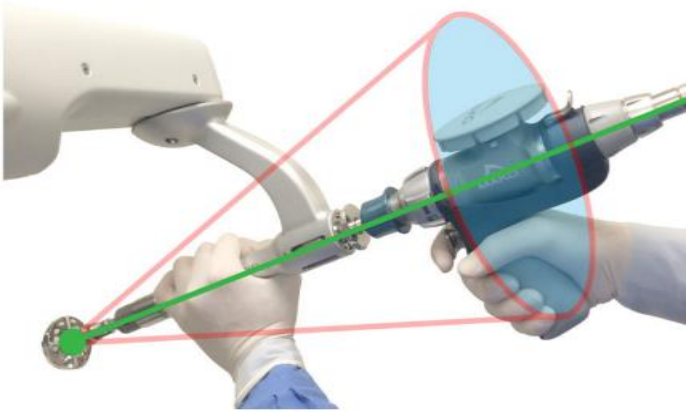

Figure 3. 4-: Initial reaming with the tip of the reamer constrained and the trajectory constrained

[MAKO THA Surgical Guides]

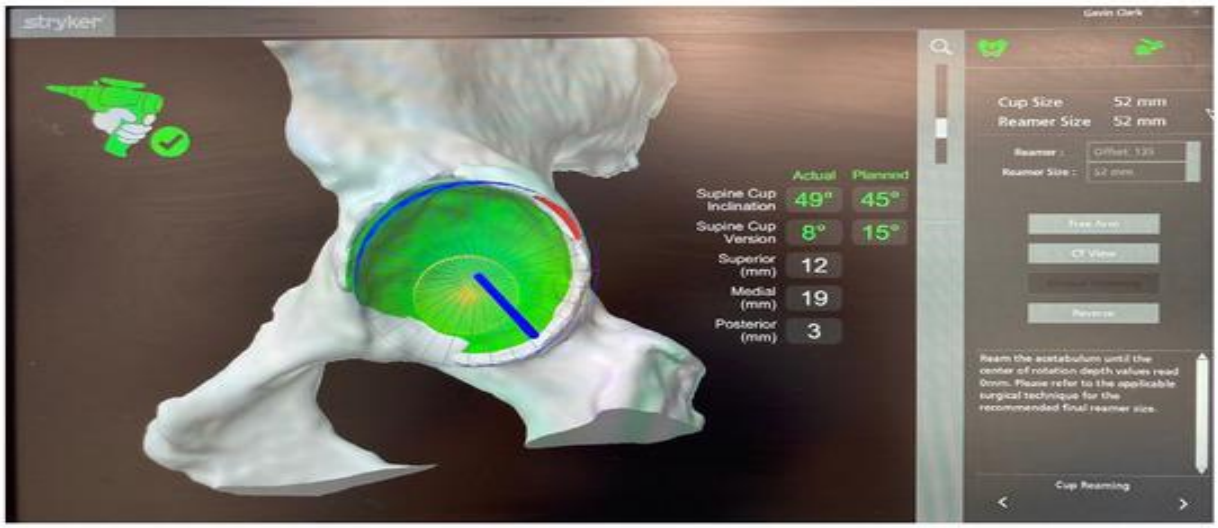

Figure 3. 5 - Intra-operative images detailing acetabular reaming relative to pre-operative plan

The blue areas indicate the reamer position. The green area is the area to be reamed, and the red area denotes minimal deviation from pre-operative plan (any further and the system would shut off), and the numbers in white indicate real-time distance from pre-operative plan as the operator reams [3].

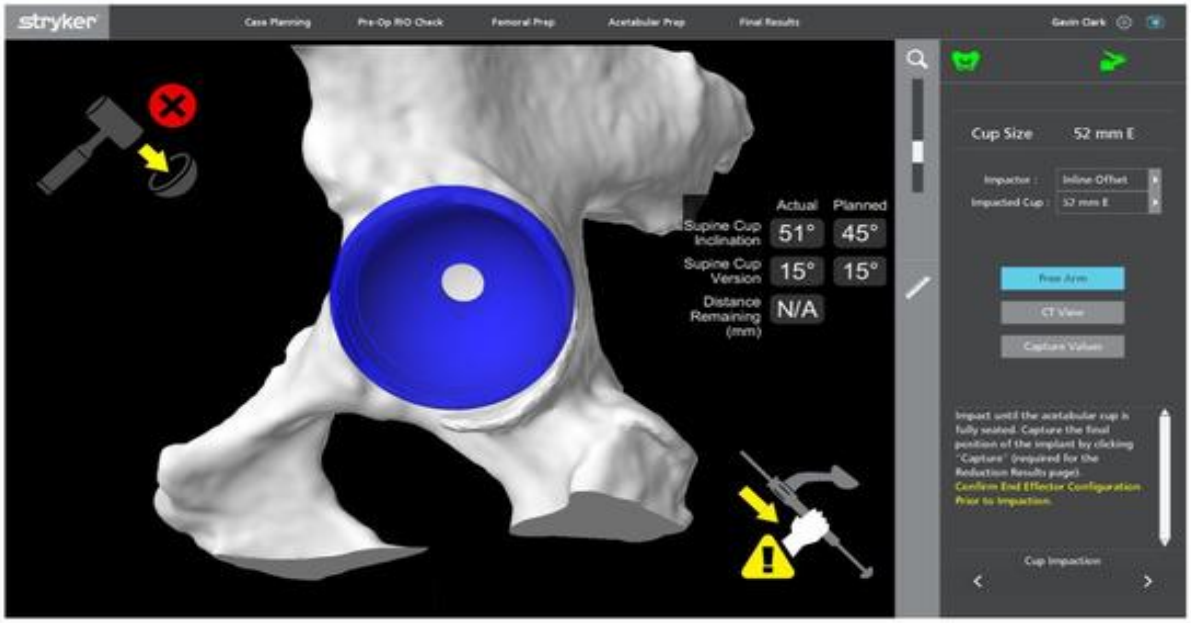

Figure 3. 6 - After reaming, the acetabular cup is accurately positioned within the acetabulum [3]

3.3.5 Broaching

Broaching involves shaping the femoral canal to fit the femoral stem of the implant. The hip end effector facilitates the insertion and alignment of the broach, transmitting the necessary forces to prepare the canal. The modular design of the effector allows for the use of different broach sizes and configurations, accommodating variations in patient anatomy.

3.3.6 Impaction

Impaction is the process of seating the acetabular and femoral components into the prepared bone cavities. The hip end effector transmits controlled, high-magnitude forces to ensure proper seating of the implants. The embedded sensors provide feedback on the forces applied, allowing for adjustments to prevent over-impaction, which could lead to bone fractures or implant damage.

3.4 Impaction Mechanics and Load Transmission Dynamics

is one of the most mechanically intensive phases in total hip arthroplasty (THA), requiring the transmission of high-magnitude, controlled forces to drive the prosthetic components—namely the acetabular cup and femoral stem—securely into their respective bone cavities. The success of this process is critically dependent on the hip end effector's ability to manage and transmit these forces without deviation, energy loss, or damage to surrounding anatomical structures. Proper impaction ensures the implant is seated with appropriate press-fit stability, which is vital for initial fixation and long-term osseointegration. The design of the end effector, therefore, plays a central role in ensuring the fidelity and safety of force delivery during this phase.

A fundamental requirement for effective impaction is the precise alignment of the end effector with respect to the implant insertion axis. Proper alignment ensures that the transmitted axial forces act uniformly along the intended anatomical pathway, typically aligned with the femoral or acetabular axes. If the effector or instrument is even slightly misaligned, the resultant vector of force may introduce lateral stress or shear forces, leading to off-axis insertion, bone microfracture, or improper implant seating. Misalignment also increases the risk of malposition, which can compromise implant stability, alter biomechanics, and accelerate wear over time. To address this, the effector incorporates mechanical features such as self-centering guide tracks, calibrated alignment pins, or robotic pose feedback systems to maintain a strict spatial orientation throughout the impaction event. The robotic control system continuously verifies this alignment using preoperative planning data, and if necessary, corrects the trajectory before the force is applied.

Another critical factor in the successful transmission of impaction forces is the material composition and structural design of the hip end effector. The components must be constructed from materials that exhibit high compressive strength, fatigue resistance, and stiffness. Titanium alloys and high-grade stainless steel are typically used due to their favorable mechanical properties and resistance to deformation under dynamic loads. During impaction, forces as high as 2,000–5,000 newtons can be generated, especially when seating large implants or compensating for dense cortical bone. The internal frame of the end effector must not flex, bend, or absorb energy in a way that diminishes the intended impulse to the implant. Finite element modeling (FEM) is often employed in the design phase to ensure that stress concentrations are minimized, and that load paths are optimized. Additionally, the effector often includes elastomeric inserts or mechanical

dampers that can modulate the transmission of peak forces, protecting both the implant and patient tissue from sudden impact surges.

Crucially, the modern hip end effector is also equipped with integrated sensor systems that provide real-time feedback on force magnitude, direction, and displacement during impaction. These may include piezoelectric force sensors, strain gauges, or capacitive load cells embedded within the effector structure. Sensor feedback serves multiple purposes: it allows the robotic system to verify that the applied force matches the pre-specified parameters, it helps detect premature seating or excessive resistance, and it can confirm that the implant has been fully seated by analyzing load-displacement trends. For example, a decreasing displacement response despite increasing applied force may indicate that full seating has been achieved. Additionally, this feedback loop enables dynamic force modulation—if the system detects excessive resistance or misalignment, it can halt impaction or adjust force application before damage occurs. In some systems, auditory or visual cues are provided to the operating surgeon based on sensor readings, further enhancing control and situational awareness during this critical step.

Taken together, the alignment precision, material engineering, and sensor feedback of the hip end effector form a synergistic system that ensures controlled and effective load transmission during implant impaction. These design considerations are essential not only for improving surgical outcomes but also for reducing the risk of intraoperative complications. As robotic systems evolve, future end effectors may incorporate adaptive stiffness mechanisms, AI-driven force modulation, or even haptic feedback systems to further refine the impact process.

CHAPTER 4

MODELING & SIMULATION SETUP

4.1 CAD modeling of the hip end effector

Introduction

Computer-Aided Design (CAD) plays a pivotal role in the development of precise and efficient surgical instruments, particularly in orthopedic procedures like Total Hip Arthroplasty (THA). This chapter outlines the complete design and modeling of a hip end effector using **PTC Creo Parametric**, a widely adopted CAD platform. The focus is on creating a functionally robust and ergonomically sound model based on essential design components including ball bearings, chuck slide assemblies, reamer barrels, and more.

Objective

The objective of this modeling task is to design a high-precision **hip end effector** capable of accommodating the mechanical and functional requirements of reaming and implant positioning during hip surgery. The model integrates multiple critical components to ensure rotational freedom, axial alignment, and secure tool engagement.

4.2 CAD Modeling

Modeling Environment

The model was created in **PTC Creo Parametric**, a powerful 3D CAD tool suitable for parametric and surface-based modeling. Each part was first modeled independently and then assembled using appropriate constraints.

Figure 4. 1 - Side view of assembled part of Hip End Effector with Reamer

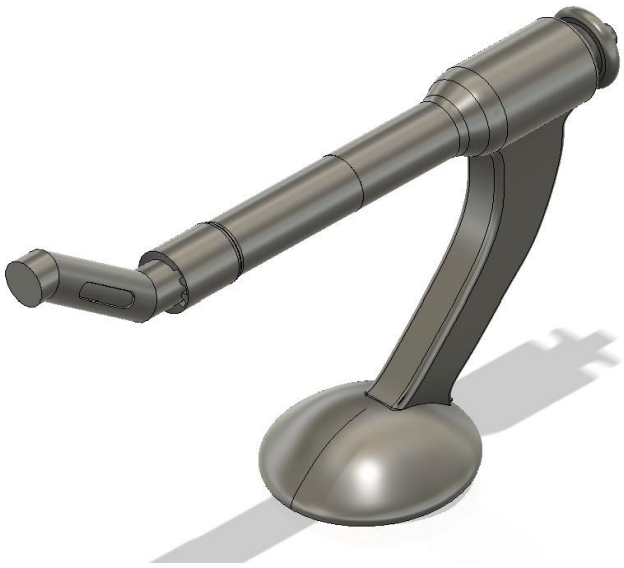

Figure 4. 2 - Assembled part of Hip End Effector with Reamer

Locking Mechanism

The locking mechanism functions by engaging interlocking splines at the joint interface, allowing the shaft to be locked at predefined angular positions and restricting rotational movement. A orientation pin is inserted through the elongated slot on the outer shaft and into a corresponding hole or groove in the inner shaft, secures the joint axially. By rotating the inner shaft to align different spline teeth, the joint can be locked at various discrete angles, enabling adjustable but secure positioning.

Figure 4. 3 - Locking Mechanism with Internal Spline Engagement

Figure 4. 4 - Locking Mechanism with Spline Engagement and Guide Slot

Compression Spring

A **compression spring** with **0.85 mm diameter** and **15 mm length** is mounted behind the release knob to provide resistance force and return it to its neutral position automatically.

Figure 4. 5 - Compression Spring

Figure 4. 6 - Spring placement within Hip Chuck Slide Assembly

Release Knob

The **Release Knob**, with a **diameter of 37.5 mm**, serves as the manual locking mechanism. It is ergonomically designed for quick engagement and disengagement of the surgical tool with minimal torque.

Figure 4. 7 - Release Knob

Hip Chuck Slide Assembly

The **Hip Chuck Slide Assembly** has a **total length of 75.88 mm** and is responsible for translating the axial motion into a locking action.

Figure 4. 8 - Hip Chuck Slide Assembly

Reamer Barrel

With an **outer diameter of 37.77 mm**, the reamer barrel accommodates various femoral head sizes. It is structurally reinforced and designed to securely house the reaming bit.

Figure 4. 9 - Reamer Barrel

Impaction platform

The central **shaft (reamer)** within the end effector shows a variable internal diameter ranging from **10.56 mm to 19 mm**. The shaft's **total length is 266.42 mm**, optimized for surgical reach and compatibility with standard reaming tools.

Figure 4. 10 - Impaction Platform

4.3 Finite Element Modelling

Introduction

This chapter presents a comprehensive overview of the modeling assumptions, boundary conditions, material properties, and simulation setup used to analyze the redesigned hip end effector for orthopedic surgical applications. The simulation is conducted using ANSYS Workbench 2024 R2, specifically within the Static Structural module. The focus lies in understanding the von Mises stress distribution and total deformation under axial loading conditions of 5000 N and 7500 N for the following materials including Cobalt Alloy, Titanium Alloy (Ti-6Al-4V) and 17- 4 PH Stainless Steel.

Importing Geometry for FEM Analysis

The model was created in accordance with the geometric modeling section using Creo and then imported as an IGES file from the CAD software for further processing.

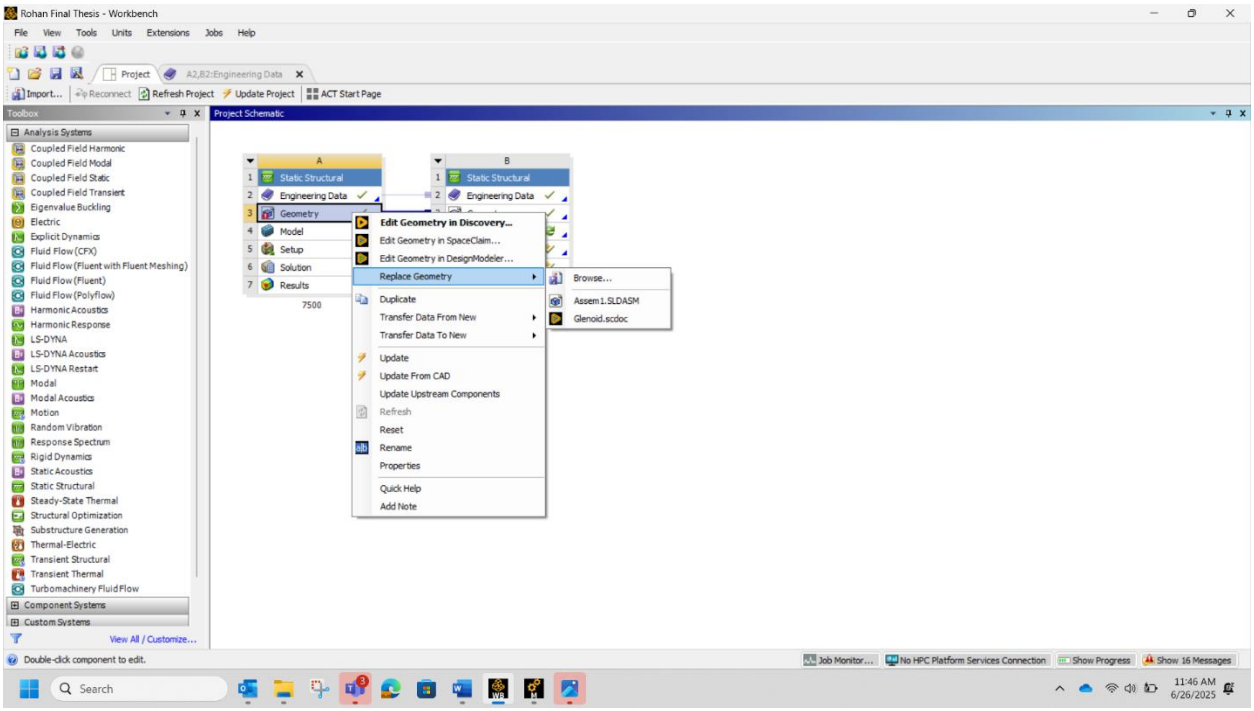

Figure 4. 11 - Importing Geometry

Material Properties Used

The following material properties were defined for simulation, based on literature and standard databases:

Common Advantages Across All Three Materials

- **High Biocompatibility**
  All three materials are well-tolerated by the human body, making them suitable for surgical tools and long-term implants. They do not cause toxic or inflammatory responses, which is crucial for medical applications.
- **Excellent Mechanical Performance**
  These materials exhibit a combination of strength, stiffness, and durability, making them capable of withstanding the mechanical demands of surgical procedures and physiological loading conditions.
- **High Mechanical Strength**
  It provides the necessary toughness and hardness required for surgical instruments and end effectors that encounter impact and repeated use.
- **Corrosion Resistance**
  Offers resistance to bodily fluids and sterilization processes, ensuring reliability and longevity.**: -** In the Engineering Data section, material properties will be established for the five materials after conducting research. The engineering data will be created by defining each new material and incorporating the necessary material properties.

Property	Value
Young's Modulus	200 GPa
Density	7,750 kg/m³
Tensile Strength	0.25 Gpa
Poisson's Ratio	0.29~0.3

Table 4. 1 - Properties for 17-4 PH Stainless Steel

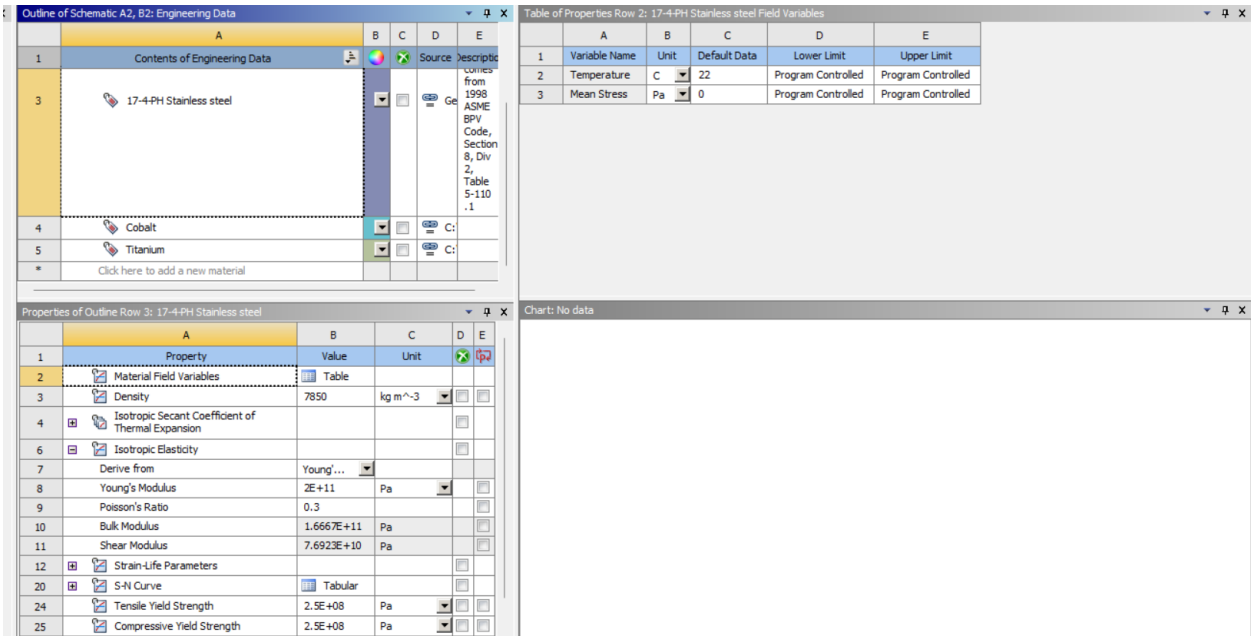

Figure 4. 12 - Assigning material properties for 17-4 PH Stainless Steel

Property	Value
Young's Modulus	0.828 GPa
Density	4500 kg/m³
Tensile Strength	0.434 GPa
Poisson's Ratio	0.3

Table 4. 2 - Properties for Titanium Alloy

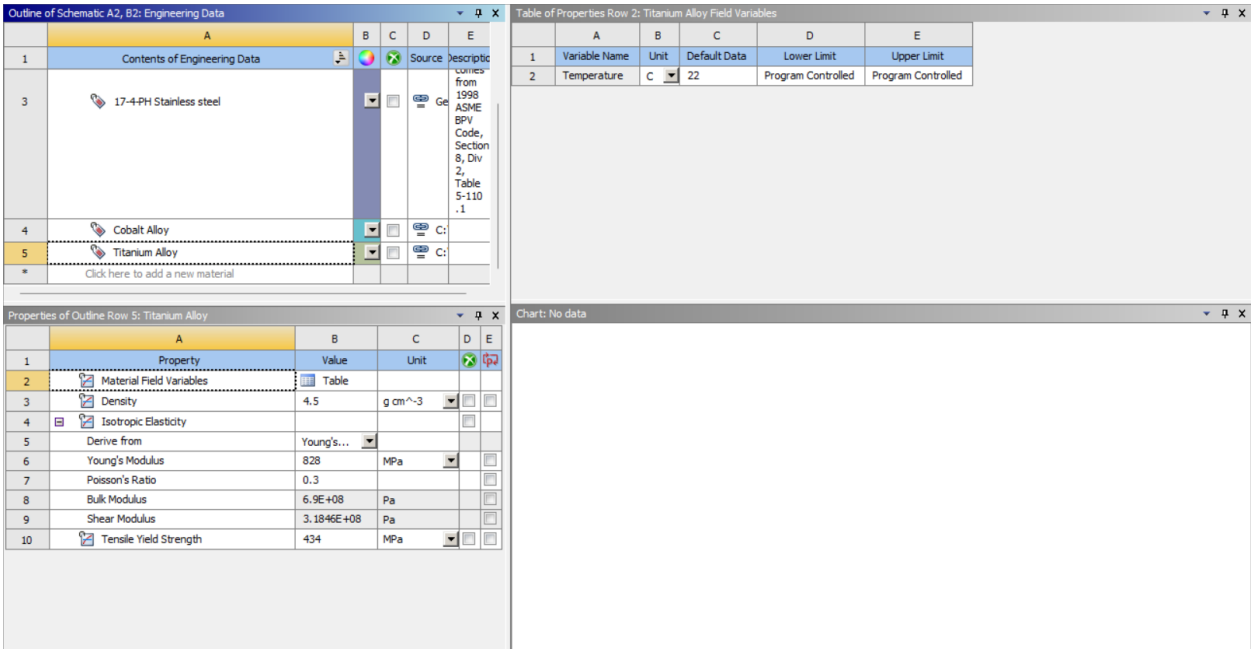

Figure 4. 13 - Assigning material properties for Titanium Alloy

Property	Value
Young’s Modulus	0.220 GPa
Density	8660 kg/m³
Tensile Strength	0.220 GPa
Poisson’s Ratio	0.33

Table 4. 3 - Properties for Cobalt Alloy

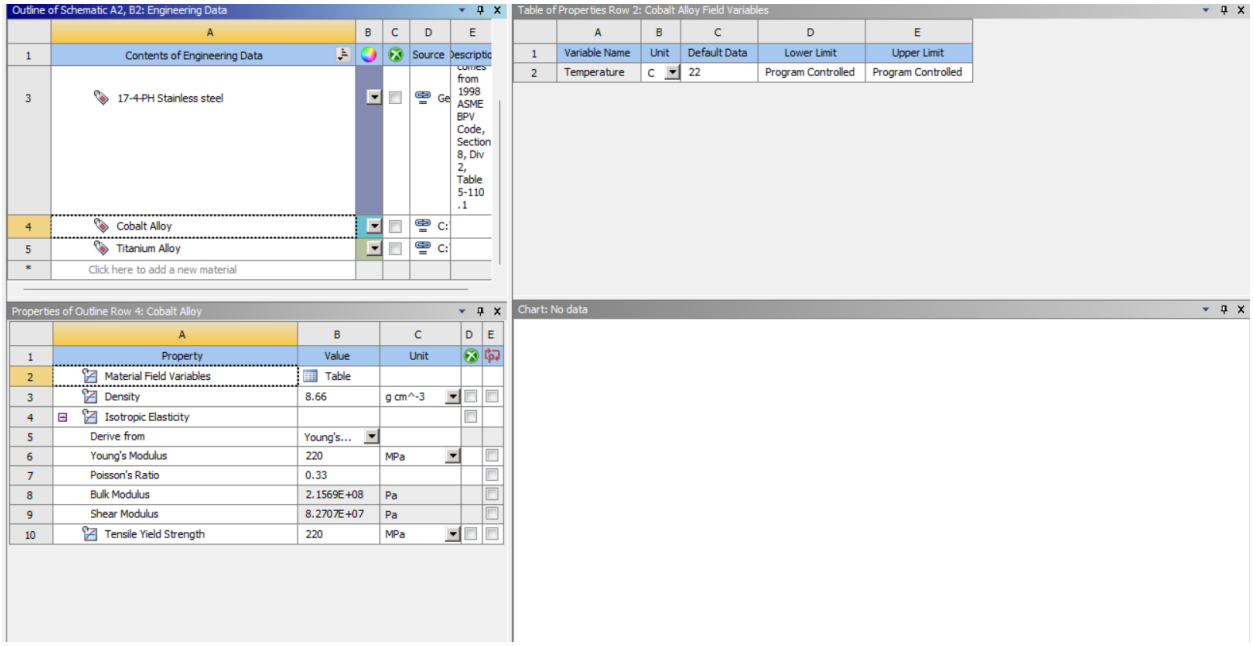

Figure 4. 14 - Assigning material properties for Cobalt Alloy

4.4 Boundary Conditions

The following boundary conditions were applied to the FEA model in ANSYS:

1. **Fixed Support:** A fixed support condition was applied to the handle end of the hip end effector. This simulates the surgeon holding the instrument rigidly during the procedure, preventing any translational or rotational movement at that point.
2. **Applied Loads:** Two axial loading scenarios were simulated at the distal end of the hip end effector, representing typical forces experienced during bone reaming and implant insertion:
    - **Load Case 1**: A force of **5000N** applied axially at the working tip.
    - **Load Case 2**: A force of **7500N** applied axially at the working tip.

These forces were distributed uniformly over the contact area at the distal end to simulate the interaction with the reamer or implant. The direction of the force was aligned with the operational axis of the tool.

4.5 Meshing Details (Element Size, Type, Quality)

Meshing is a critical step in Finite Element Analysis (FEA), as it discretizes the continuous geometry of the hip end effector into a finite number of interconnected elements. The quality and characteristics of the mesh directly impact the accuracy and computational efficiency of the simulation results**.**

Figure 4. 15 - Default Meshing

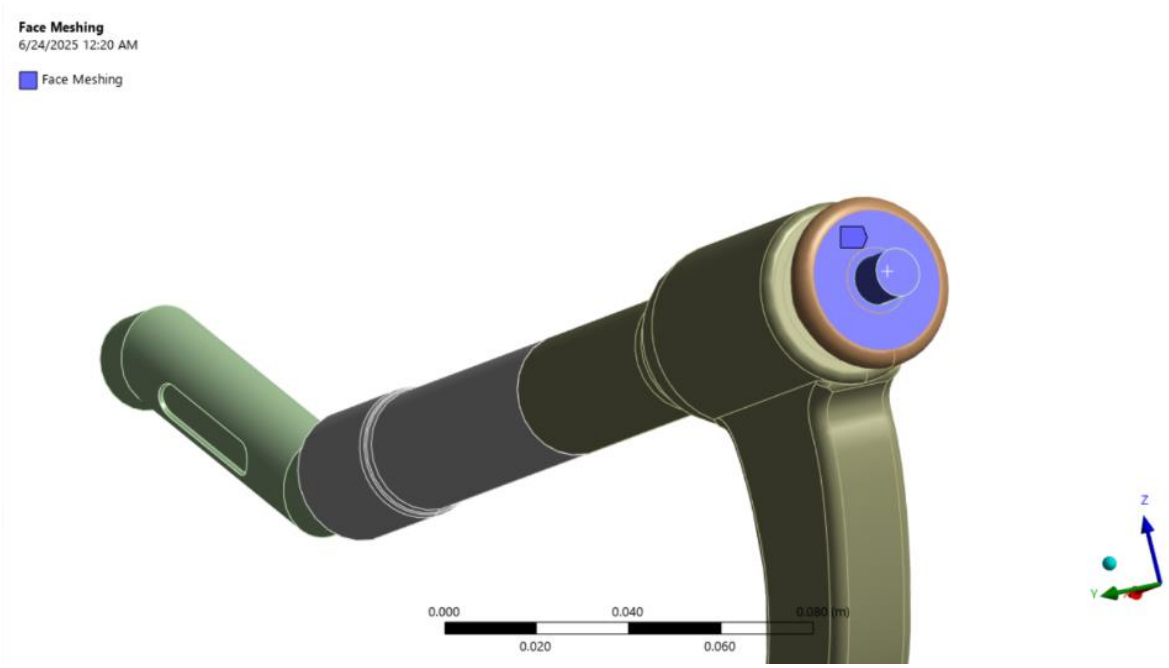

Figure 4. 16 - Face meshing

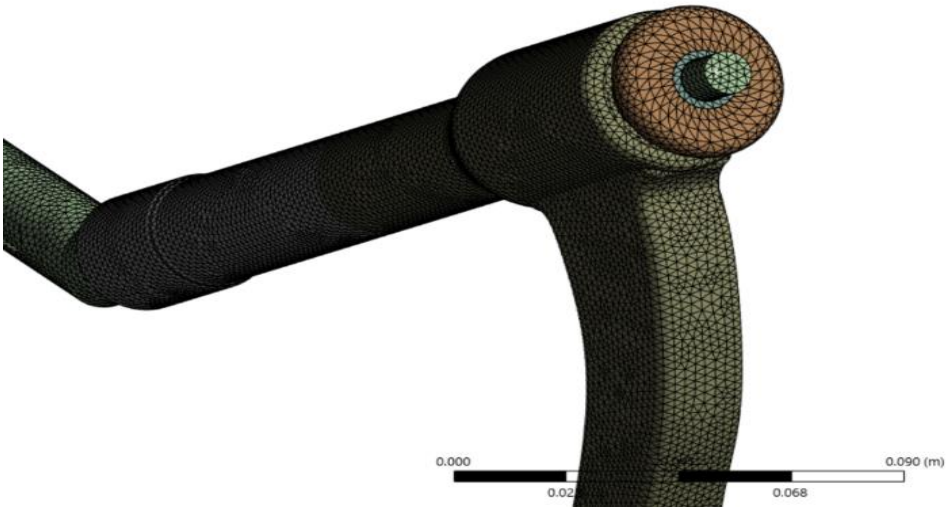

Figure 4. 17 - Refined Meshing

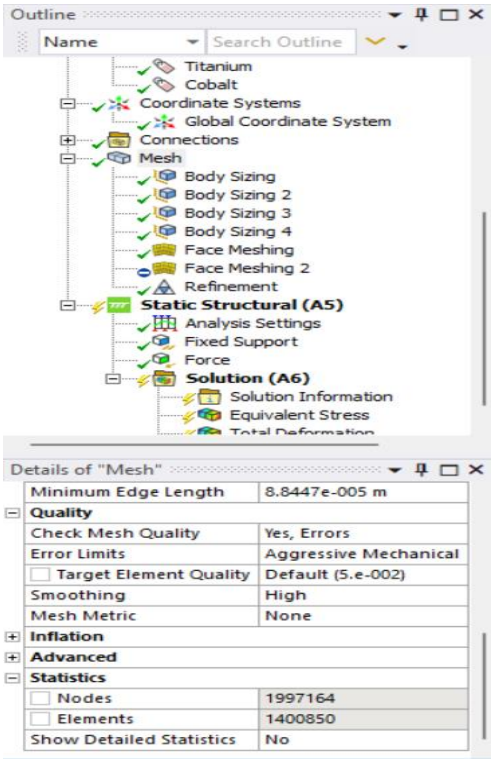

Figure 4. 18 - Details of Refined Meshing

The figures provide a clear visual representation of the meticulous meshing process undertaken for the hip end effector within the Finite Element Analysis (FEA) framework.

Element Size

The meshing process begins by discretizing the intricate geometry of the hip end effector into a vast network of smaller elements and nodes. The first image (Fig 4.15) presents the initial global mesh, characterized by 643,161 nodes and 420,519 elements, which forms the fundamental basis for the structural analysis. To achieve optimal computational efficiency and accuracy, the "Element Size" is carefully controlled and varied across the model. Advanced mesh controls such as "Body Sizing" and overall "Refinement" are employed to manipulate element dimensions. In the initial meshing pass, the global mesh was generated using program-controlled defaults for element order, refinement levels, and smoothing algorithms. However, for subsequent fine meshing of critical regions, the element formulation was explicitly set to **quadrilateral elements**, and their polynomial order was elevated from **linear (Order 1) to cubic (Order 3)**. Concurrently, a more aggressive **refinement level** was applied, transitioning from an initial setting of 1 to a higher density setting of 3, and more robust mesh smoothing algorithms were employed to enhance overall element quality and geometric conformity. This is particularly evident in the highly detailed views (Fig 4.18), where specific surfaces and volumes, likely critical regions such as attachment points or areas where high stresses are anticipated, exhibit significantly smaller elements. The "Minimum Edge Length" parameter, often defined during mesh generation, dictates the smallest allowed dimension for an element's side, directly influencing the local mesh density. This targeted reduction in element size in high-gradient regions is crucial, as it allows for precise capture of detailed stress and strain distributions. Ultimately, this approach leads to a refined state (Fig 4.18) with a higher total count of 1,997,164 nodes and 1,400,850 elements, signifying a denser and more accurate representation in the areas most relevant to the stress analysis under the applied 5000 N and 7500 N loads.

Element Type

While the figures do not explicitly specify the exact element types used for the volumetric discretization, the appearance of the meshed geometry, particularly for a complex 3D component

like a hip end effector, strongly suggests the use of **tetrahedral elements**. Tetrahedral elements (often 4-node or 10-node solid elements) are widely preferred for meshing irregular and complex geometries due to their flexibility in conforming to intricate shapes. The images show "Face Meshing" applied to specific surfaces (Fig 4.16); this surface meshing typically serves as the foundation upon which the 3D volume mesh is generated. The quality and distribution of these 2D surface elements directly influence the creation of well-formed 3D solid elements within the component. This chosen element type enables accurate representation of the material behavior under various loading conditions, allowing for robust stress and strain analysis.

Mesh Quality

Ensuring high "Mesh Quality" is a paramount step to guarantee the reliability and accuracy of the Finite Element Analysis results. Various parameters and checks are utilized to assess the quality of the generated mesh. These metrics are vital for preventing numerical inaccuracies or solving convergence issues. The interface also indicates the use of strict criteria, such as "Aggressive Mechanical" for error limits and "High" smoothing, which signifies a rigorous approach to optimizing element shape and connectivity. By maintaining a high standard

of mesh quality, the analysis minimizes errors stemming from poor element geometry, thereby ensuring that the predictions of stress and strain, particularly at critical points under the 5000 N and 7500 N loads for materials like 17-4 PH stainless steel, Cobalt, and Titanium, are reliable and representative of the physical behavior of the hip end effector.

4.6 Setup in ANSYS (Static Structural, Constraints, Loads)

The Finite Element Analysis (FEA) of the hip end effector was performed using ANSYS Workbench, a comprehensive simulation software. The "Static Structural" analysis system was utilized, as the primary objective was to assess the instrument's behavior under constant applied loads without considering time-dependent or inertial effects. The setup involved several key steps: importing the CAD model, defining engineering data (material properties), applying boundary conditions (constraints and loads), meshing, and solving the analysis.

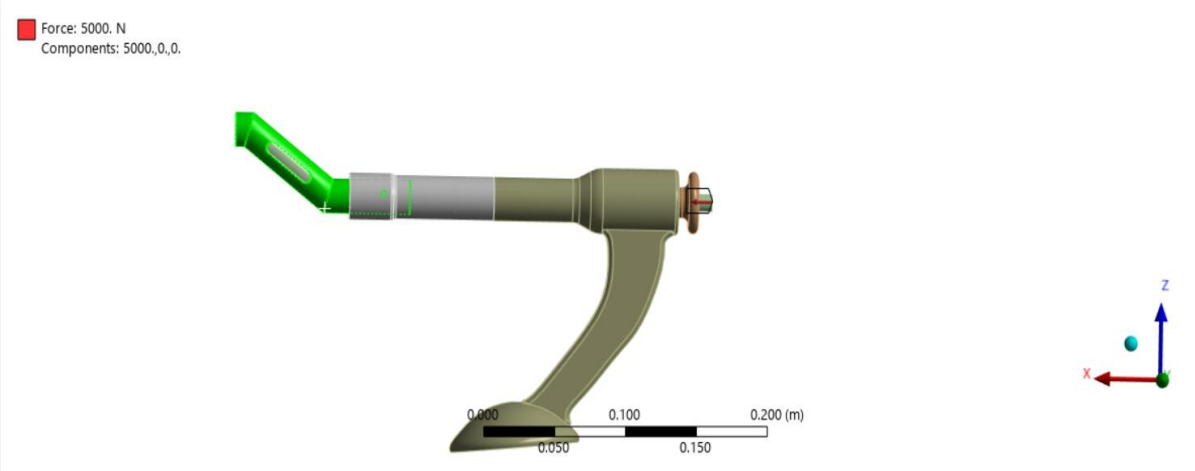

Figure 4. 19 - Boundary Conditions and Applied Load (5000 N) on the Hip End Effector

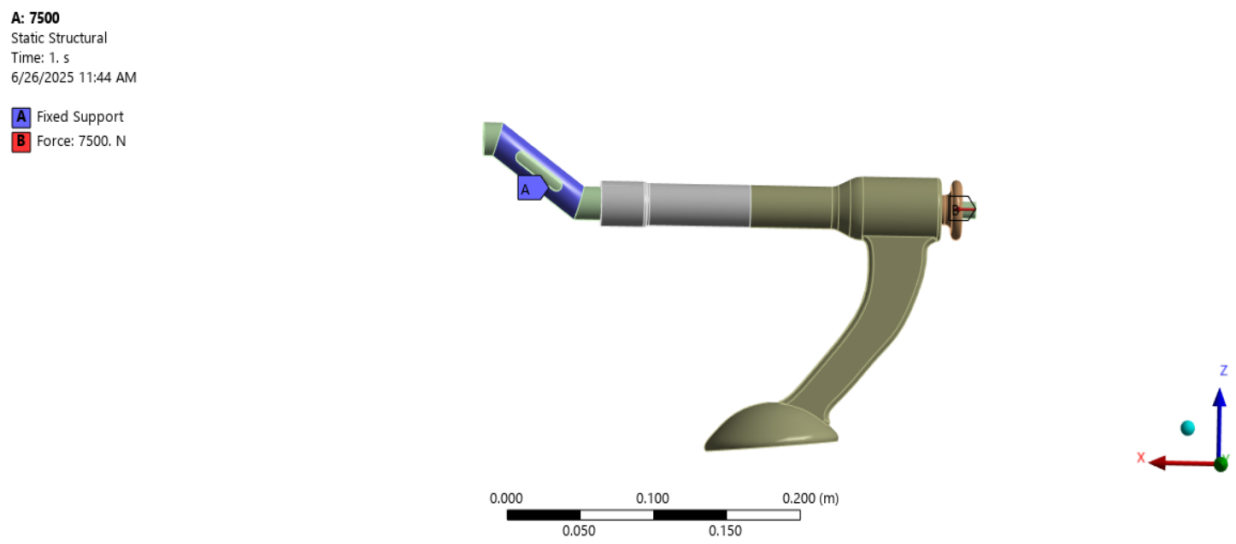

Figure 4. 20 - Boundary Conditions and Applied Load (7500 N) on the Hip End Effector

Solution

Boundary Conditions and Loads

The defined boundary conditions and loads were applied in the ANSYS Mechanical interface:

1. **Fixed Support:** A "Fixed Support" was applied to the face of the hip end effector corresponding to the handle end. This constraint prevents all translational (X, Y, Z) and rotational (around X, Y, Z) degrees of freedom at this boundary, simulating a rigid holding condition.
2. **Applied Force:** A "Force" load was applied to the circular face at the very distal tip of the hip end effector, simulating the impaction point.
    - The force was defined as an axial load, directed along the longitudinal axis of the hip end effector.
    - **Two separate axial loads were considered:**
        - **Load 1: Magnitude of 5000 N**
        - **Load 2: Magnitude of 7500 N**

      The force was applied to ensure correct directionality and was set to act perpendicularly to the contact surface.

CHAPTER 5

RESULTS AND DISCUSSION

This chapter presents and discusses the results obtained from the finite element analysis (FEA) performed on the designed component. The analysis focused on understanding the component's structural integrity under specified loading conditions, specifically examining von Mises stress distribution, total deformation (strain), and identifying critical load paths. Three primary materials, Cobalt, Titanium, and 17-4 PH Stainless Steel, were evaluated to compare their performance characteristics.

Load Case 1: 5000 N

5.1 Stress Analysis: Von Mises Stress Regions and Critical Locations at 5000 N

The von Mises equivalent stress criterion was employed to assess the yielding potential of the materials under complex loading. This criterion provides a single, positive stress value that can be compared against the material's yield strength. Higher von Mises stress indicates areas more prone to yielding.

5.1.1 17-4 PH Stainless Steel Material Analysis

For the 17-4 PH Stainless Steel component, the maximum von Mises stress, as depicted in **Figure 5.1**, was found to be approximately **111.89 MPa**.

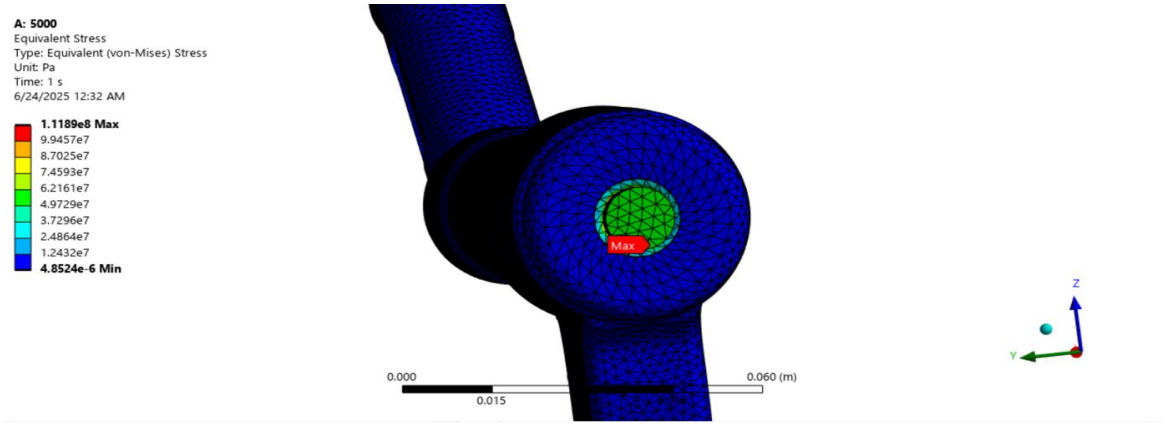

Figure 5. 1 - Von Mises Stress Distribution for 17-4 PH Stainless Steel Component under 5000 N

- The critical locations for the 17-4 PH Stainless Steel component were observed at the interface region where the main cylindrical body connects to the base/support structure.
- Localized stress concentrations on the inner cylindrical surface at the connection point to the fixed support.

5.1.2 Titanium Material Analysis

For the Titanium component, the maximum von Mises stress, as depicted in **Figure 5.2** & **Figure 5.3**, was found to be approximately **111.89 MPa**.

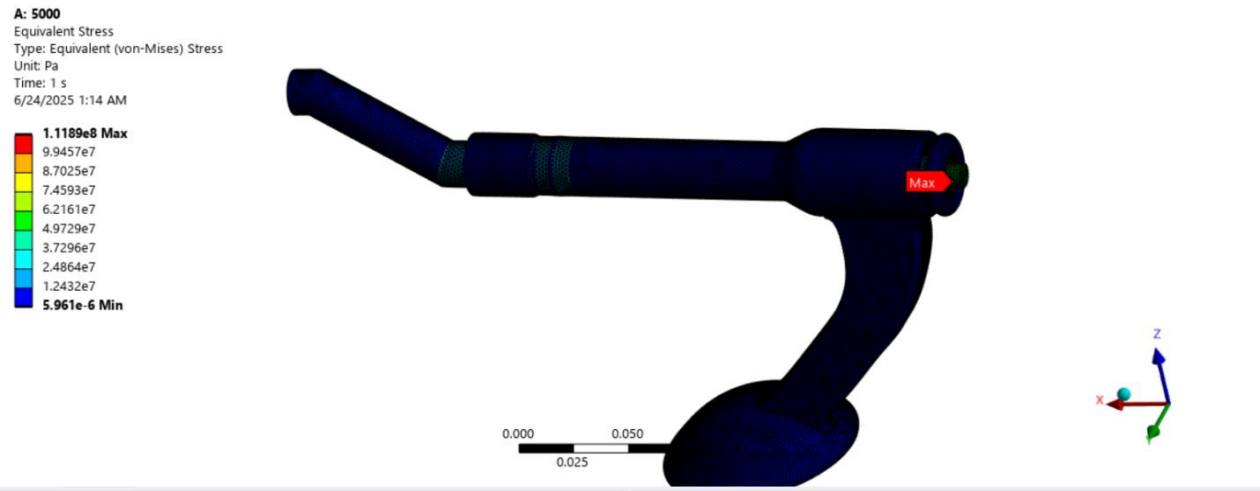

Figure 5. 2 - Von Mises Stress Distribution for Titanium Alloys under 5000 N

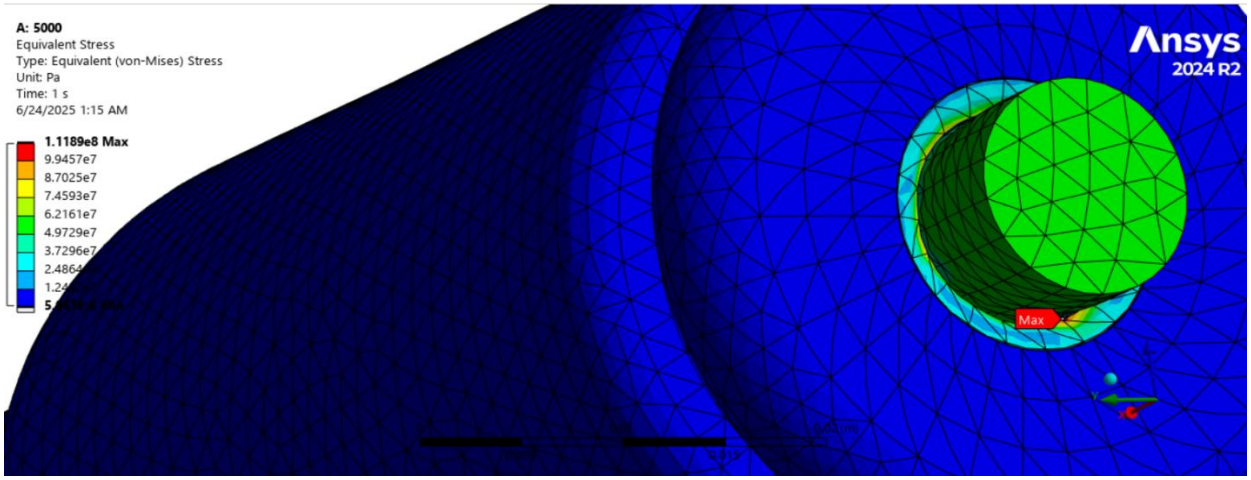

Figure 5. 3 - Von Mises Equivalent Stress distribution showing the maximum stress region (red) in the component under 5000 N

The critical locations for the Titanium component were identified at:

- The same interface region between the main cylindrical body and the base, particularly at the point of load transfer to the fixed support.

5.1.4 Cobalt Material Analysis

As shown in **Figure 5.4** & **Figure 5.5** the maximum von Mises stress observed in the Cobalt component was approximately **109.83 MPa**.

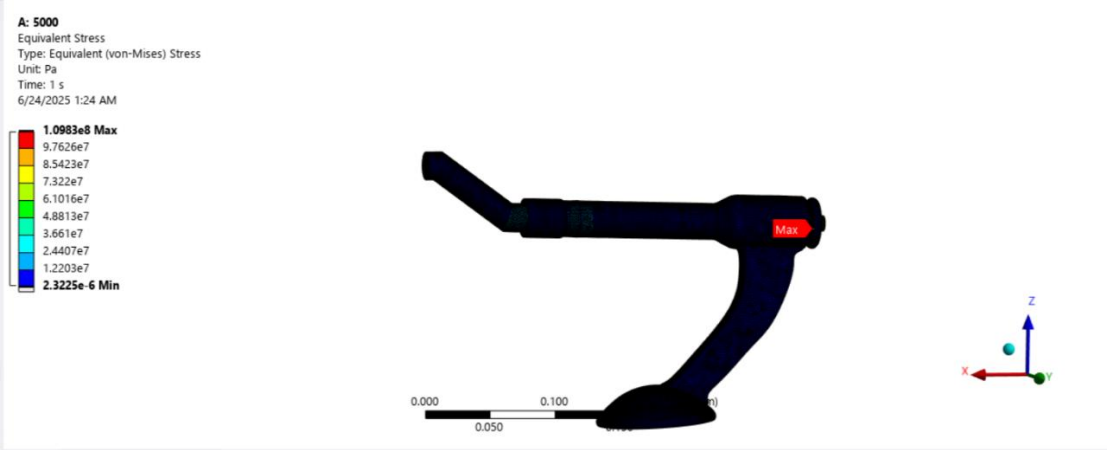

Figure 5. 4 - Von Mises Stress Distribution for Cobalt Component under 5000 N

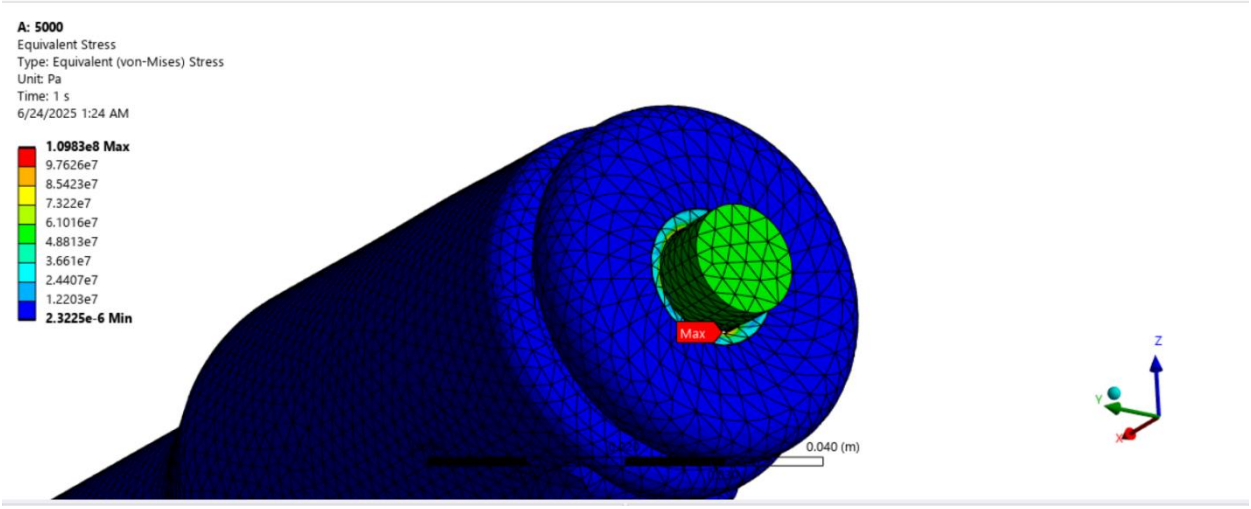

Figure 5. 5 - Von Mises Equivalent Stress distribution for Cobalt Component showing the maximum stress region (red) in the component under 5000 N

The critical locations, characterized by the highest stress concentrations (indicated by red regions in the stress contour plot), were consistently found at:

- The interface region where the main cylindrical body connects to the base/support structure. This area experiences significant stress due to the transition in geometry and the transfer of load from the cantilevered arm to the fixed support.
- Specifically, a localized stress concentration was observed on the inner cylindrical surface at this connection point, suggesting a high bearing or shear stress.

  These regions are critical as they are the most likely points for material yielding or fatigue failure under repeated loading.

Discussion on Stress Analysis

A comparison of the stress results reveals that Cobalt and Titanium components experience similar maximum von Mises stress values, with Titanium showing a slightly lower peak stress. Based on typical material properties, 17-4 PH Stainless Steel is also expected to exhibit comparable stress distribution patterns, with peak stresses occurring at the same critical locations due to the identical geometry and loading conditions. The specific magnitude for 17-4 PH Stainless Steel will depend on its elastic properties. The choice among these materials would depend on their respective yield strengths, fatigue properties, as well as cost, weight, and environmental considerations, relative to these observed peak stress values.

5.2 Total Deformation Analysis Under Load and Safe Limits at 5000 N

Total deformation analysis provides insight into how much the component displaces under the applied load, which is crucial for assessing its functional integrity and ensuring it remains within acceptable operational limits.

5.2.1 17-4 PH Stainless Steel Material Analysis

For the 17-4 PH Stainless Steel component, the total deformation is presented in **Figure 5.6** & **Figure 5.7**. The maximum total deformation was approximately **2.0147 x 10^-5 m.**

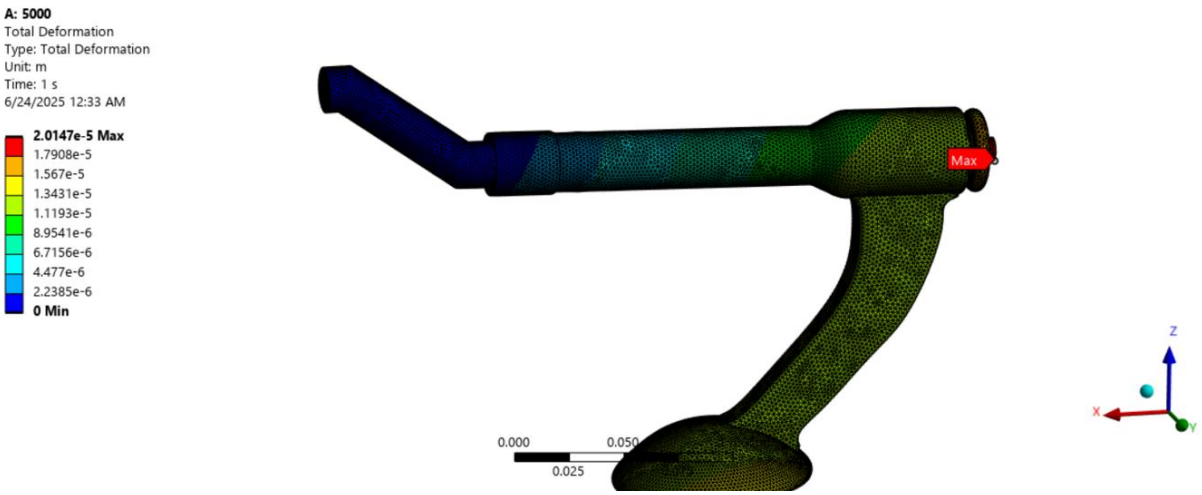

Figure 5. 6 - Total Deformation for 17-4 PH Stainless Steel Component under 5000 N

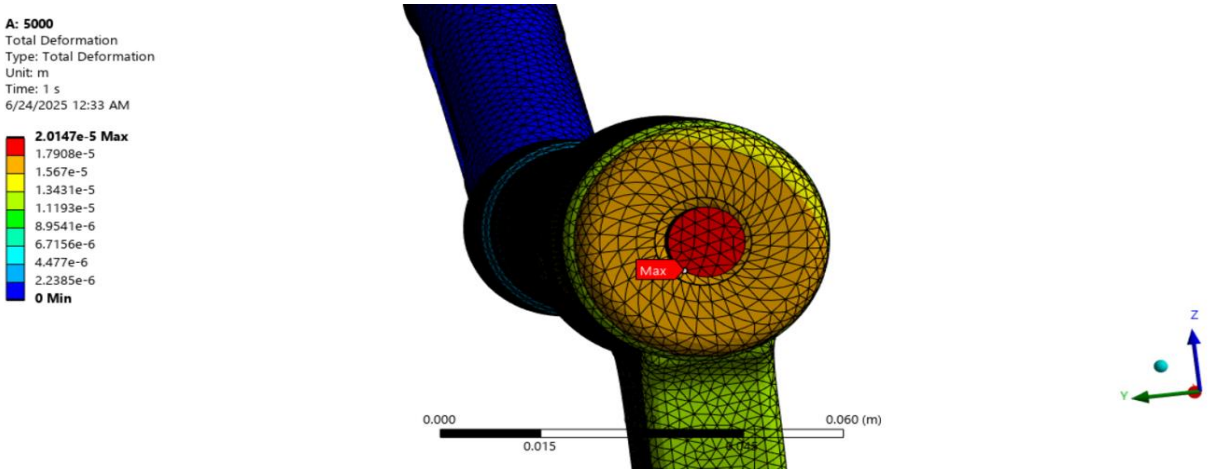

Figure 5. 7 - Total Deformation plot of the 17-4 PH Stainless Steel component under a 5000 N load, indicating a maximum deflection

As with the other materials, the maximum deformation for 17-4 PH Stainless Steel was concentrated at the free end of the cantilevered arm, diminishing towards the fixed support.

5.2.2 Titanium Material Analysis

For the Titanium component, the total deformation is presented in **Figure 5.8** The maximum total deformation was significantly higher, approximately **0.0048666 m**.

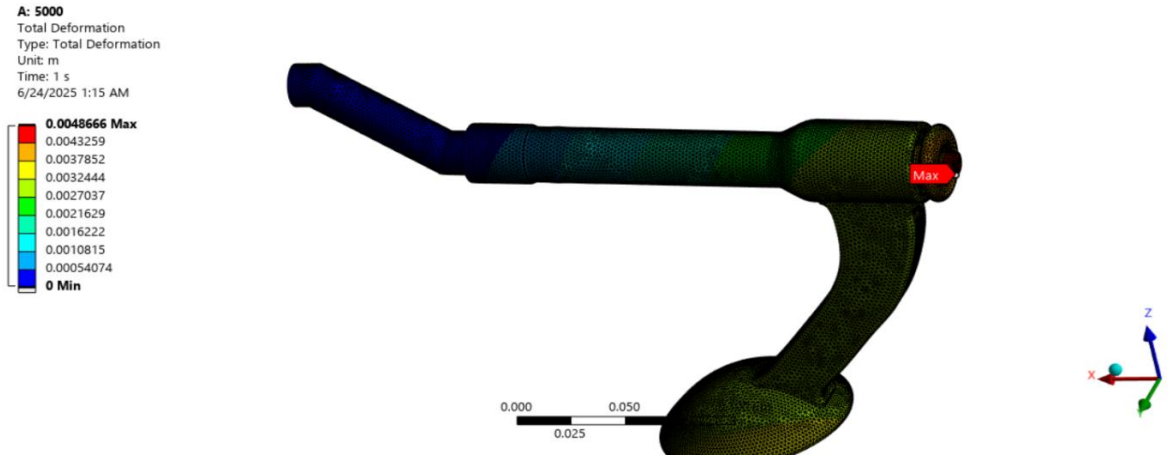

Figure 5. 8 - Total Deformation for Titanium Component under 5000 N

The maximum deformation was concentrated at the free end of the cantilevered arm.

5.2.3 Cobalt Material Analysis

The total deformation of the Cobalt component is illustrated in **Figure 5.9** & **Figure 5.10** the maximum total deformation recorded was approximately **0.018237 m.**

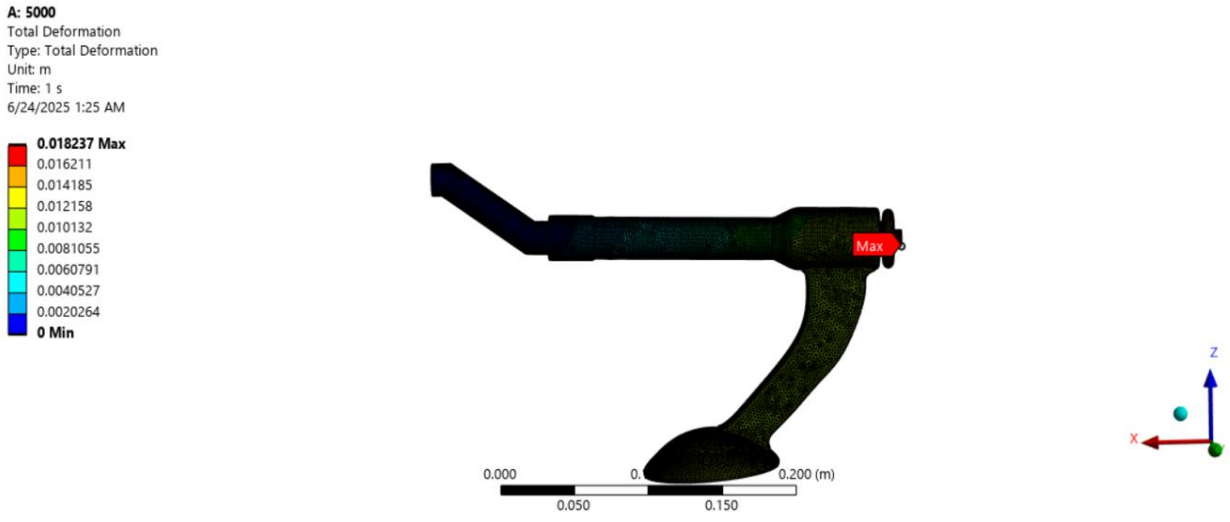

Figure 5. 9 - Total Deformation for Cobalt Component under 5000 N

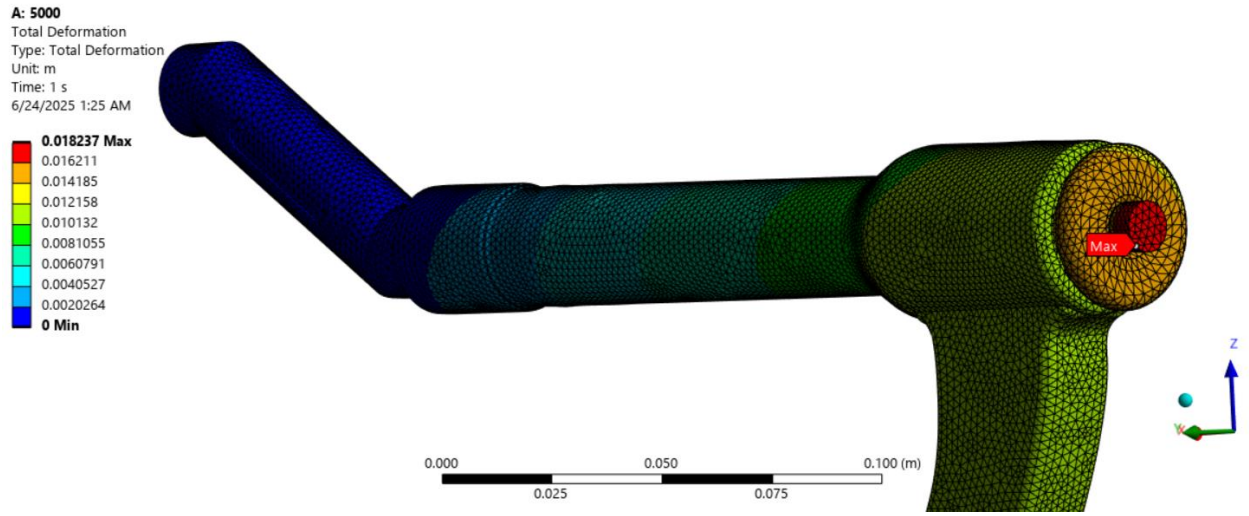

Figure 5. 10 - Total Deformation plot of the Cobalt component under a 5000 N load, indicating a maximum deflection

The highest deformation was observed at:

- The free end of the cantilevered arm, farthest from the fixed support. This is an expected outcome as this is the point with the longest lever arm relative to the fixed support, resulting in maximum deflection.

The deformation gradually decreases as one move closer to the fixed support.

Discussion on Strain Analysis and Safe Limits:

The most striking difference among the materials is evident in the total deformation results. The Titanium component exhibited a significantly larger deformation (more than 800 times) compared to the Cobalt component under the same loading conditions, indicating Cobalt's superior stiffness. 17-4 PH Stainless Steel typically possesses a Young's Modulus higher than Titanium but lower than Cobalt, suggesting its deformation will likely fall between the two, being stiffer than Titanium but less stiff than Cobalt.

The "safe limits" for deformation depend entirely on the functional requirements of the component. If high dimensional stability is required, Cobalt would be the preferred choice due to its minimal

deformation. If a certain degree of flexibility is acceptable, 17-4 PH Stainless Steel or even Titanium might be viable, provided the deformation remains within the elastic limit and does not compromise functionality. The final material selection should balance the mechanical performance (stress and strain limits) with other critical factors such as manufacturing cost, weight constraints, and specific application requirements.

5.3 Force Analysis: Load Paths

Understanding load paths is essential for optimizing component geometry and ensuring efficient transfer of forces to the supporting structures. The analysis of stress and deformation patterns allows for the inference of these paths.

The applied force is applied to the end of the extended arm with a magnitude of 5000 N. The fixed support, on the other hand, is located at the base of the component, providing the reaction forces necessary to counteract the applied load.

1. ***From Applied Force to Main Body***: The applied force at the end of the arm induces bending and shear stresses along the entire length of the arm. The load is primarily transferred axially along the arm and as a bending moment into the main cylindrical body.
2. ***Through the Main Body***: The cylindrical section of the component acts as a beam, transmitting the bending moments and shear forces towards the fixed end. The stress concentration at the interface (as seen in all stress analyses) clearly indicates this region is bearing the accumulated forces and moments before they are transferred to the support.
3. ***To the Fixed Support***: The load is finally transferred from the cylindrical body to the fixed base. The high stress concentrations at the connection points with the fixed support confirm that these are the primary load-bearing areas responsible for anchoring the component. The entire structure acts as a cantilever beam, with the load being absorbed and transferred by the material from the point of application to the point of constraint.

   The continuous nature of the stress and strain contours from the point of load application to the fixed support illustrates a clear and direct load path, which is consistent across all analyzed materials. Optimizing the geometry and material properties in these load path regions,

particularly at transitions and connection points, is crucial for enhancing the component's overall strength and durability.

Three primary materials, Cobalt, Titanium, and 17-4 PH Stainless Steel, were evaluated to compare their performance characteristics under an applied load of **7500 N**.

Load Case 2: 7500 N

5.3 Stress Analysis: Von Mises Stress Regions and Critical Locations at 7500 N

The von Mises equivalent stress criterion was employed to assess the yielding potential of the materials under complex loading. This criterion provides a single, positive stress value that can be compared against the material's yield strength. Higher von Mises stress indicates areas more prone to yielding.

5.3.1 17-4 PH Stainless Steel Material Analysis

For the 17-4 PH Stainless Steel component, the maximum von Mises stress under a **7500 N** load, as depicted in **Figure 5.11** & **Figure 5.12** was found to be approximately **167.83 MPa**.

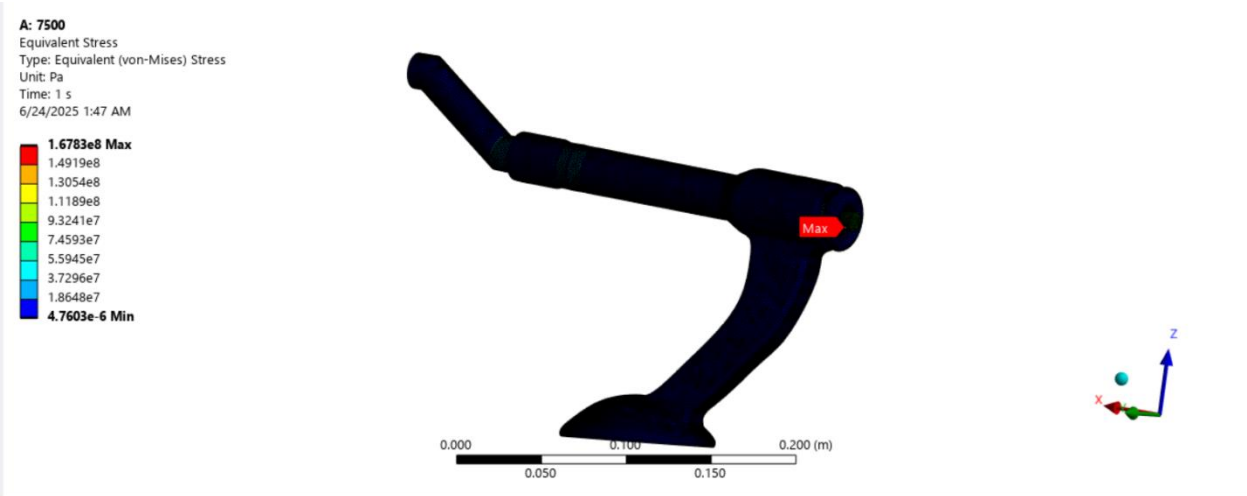

Figure 5. 11 - Von Mises Stress Distribution for 17-4 PH Stainless Steel Component

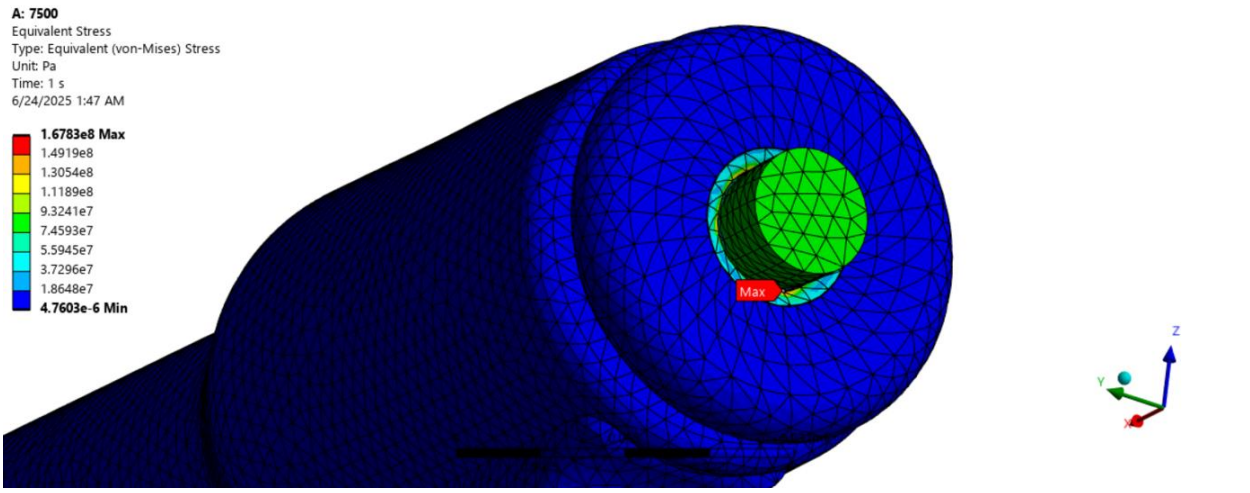

Figure 5. 12 - Von Mises Equivalent Stress distribution for 17-4 PH Stainless Steel Component showing the maximum stress region (red) in the component under 7500 N

The critical locations for the 17-4 PH Stainless Steel component were observed to be consistent with those identified for Titanium and Cobalt:

- The interface region where the main cylindrical body connects to the base/support structure.
- Localized stress concentrations on the inner cylindrical surface at the connection point to the fixed support.

5.3.3 Titanium Material Analysis

For the Titanium component, the maximum von Mises stress under a **7500 N** load, as depicted in **Figure 5.13** was found to be approximately **167.83 MPa.**

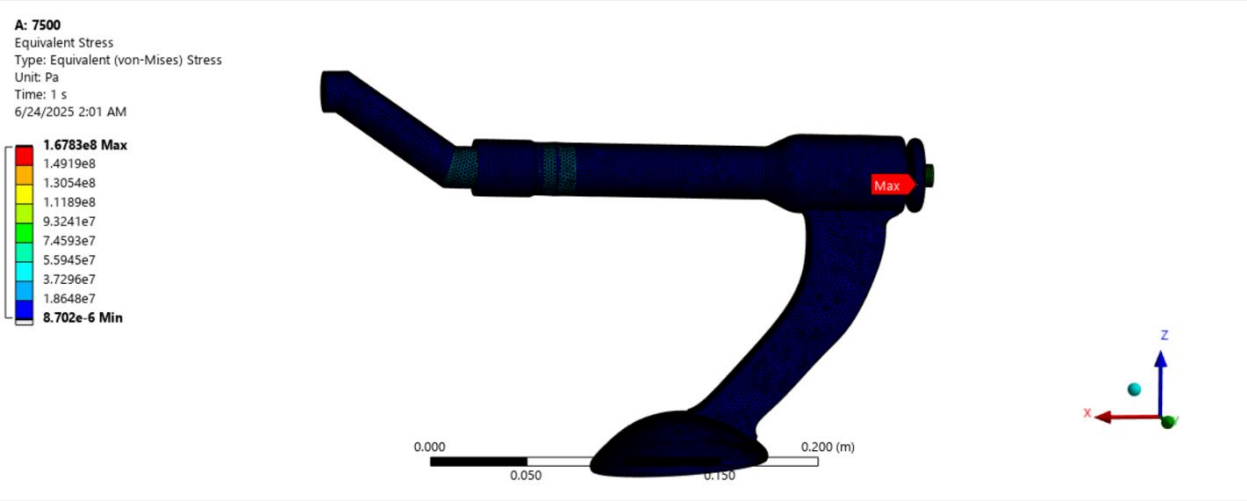

Figure 5. 13 - Von Mises Stress Distribution for Titanium Alloy Component 7500 N Load

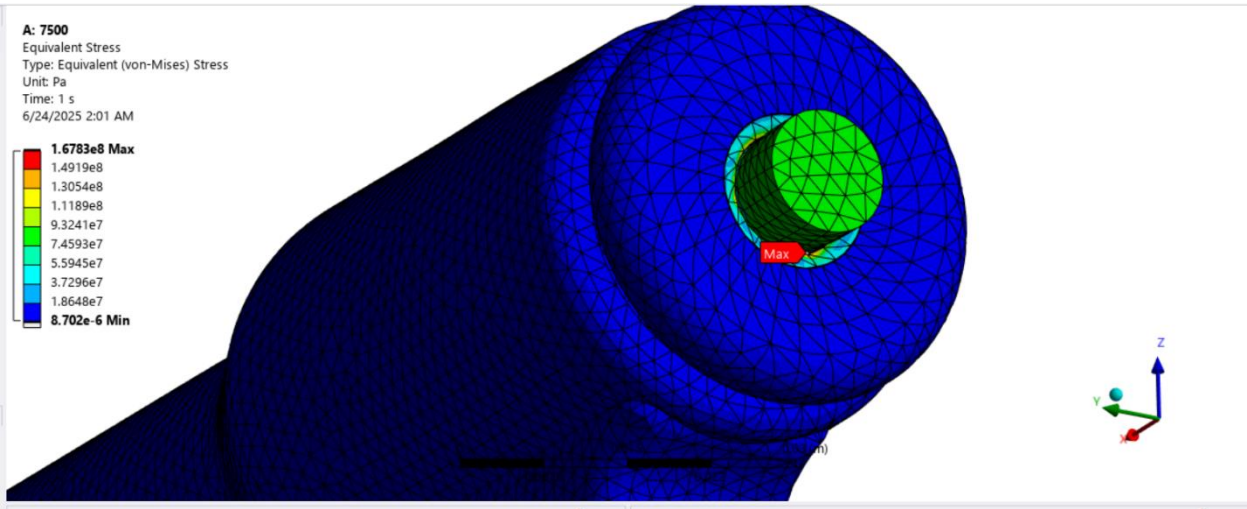

Figure 5. 14 - Von Mises Equivalent Stress distribution for Titanium Alloy Component showing the maximum stress region (red) in the component under 7500 N

Like previous analyses, the critical locations for the Titanium component were identified at:

- The interface region between the main cylindrical body and the base, particularly at the point of load transfer to the fixed support.
- The innermost circular section at this connection point also showed high stress concentration.

5.3.5 Cobalt Material Analysis

For the Cobalt component under a **7500 N** load, the maximum von Mises stress was found to be approximately **164.74 MPa**.

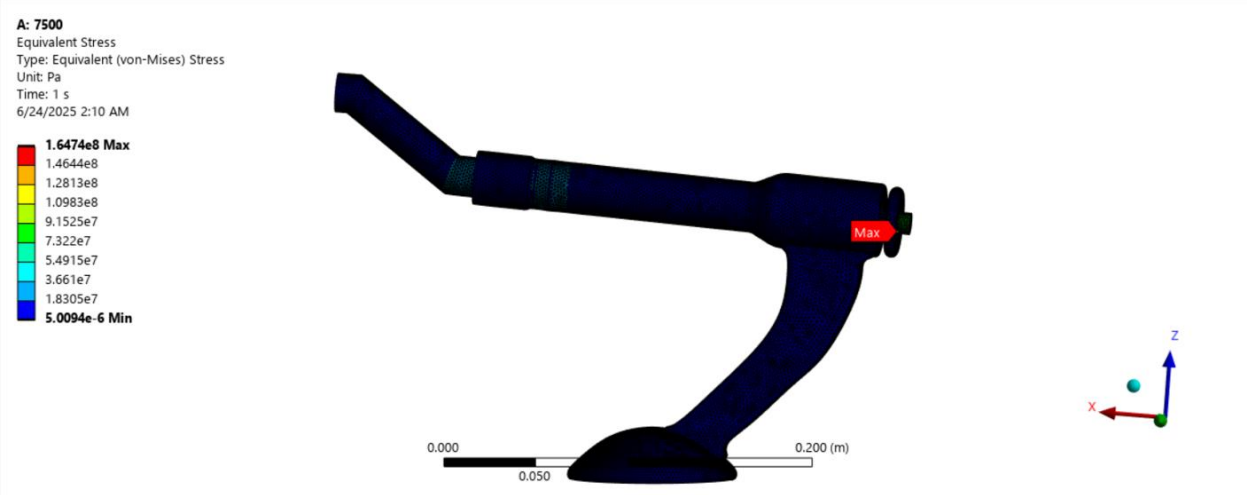

Figure 5. 15 - Von Mises Stress Distribution for Cobalt Alloy Component under 7500 N Load

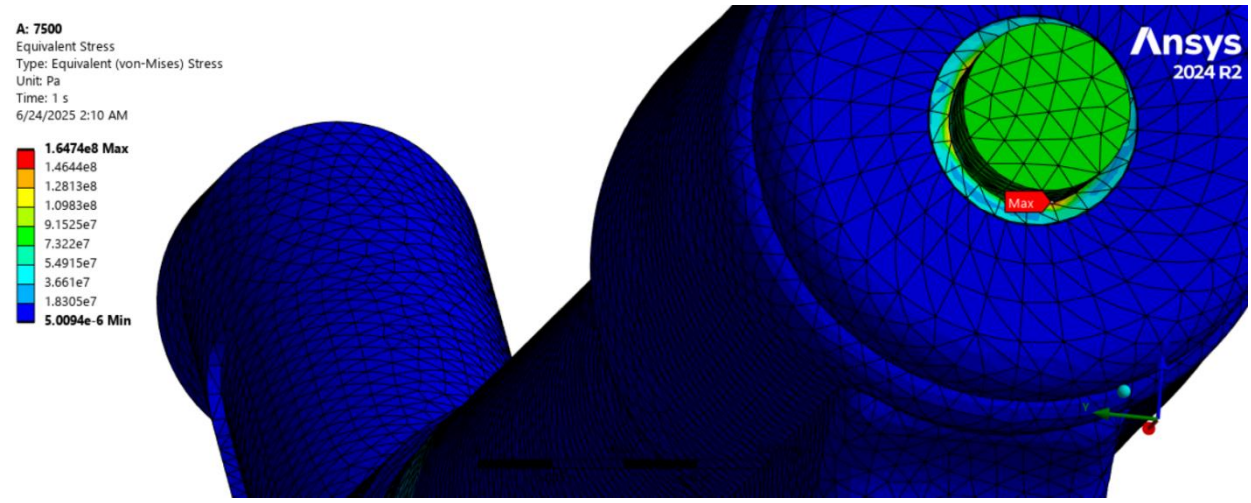

Figure 5. 16 - Von Mises Equivalent Stress distribution for Cobalt Alloy Component showing the maximum stress region (red) in the component under 7500 N

The critical locations, characterized by the highest stress concentrations, are expected to be consistent with previous analyses:

- The interface region where the main cylindrical body connects to the base/support structure.
- Localized stress concentration on the inner cylindrical surface at this connection point. These regions are critical as they are the most likely points for material yielding or fatigue failure under repeated loading.

Discussion on Stress Analysis

Under a 7500 N load, Titanium and 17-4 PH Stainless Steel components show very similar maximum von Mises stress values, approximately 167.83 MPa. This indicates that for this increased load, these materials experience comparable peak stress magnitudes and distribution patterns, with the critical areas remaining consistent at the interface with the fixed support. For Cobalt, similar stress patterns are anticipated, and its specific value will need to be provided. The general observation is that increasing the load from 5000 N to 7500 N (a 50% increase) leads to a proportional increase in peak stress values, highlighting the linear elastic behavior under these conditions. The choice among these materials would depend on their respective yield strengths relative to these peak stress values, as well as fatigue properties, cost, and weight.

5.4 Total Deformation Under Load and Safe Limits at 7500 N

Total deformation analysis provides insight into how much the component displaces under the applied load, which is crucial for assessing its functional integrity and ensuring it remains within acceptable operational limits.

5.4.1 17-4 PH Stainless Steel Material Analysis

For the 17-4 PH Stainless Steel component, the total deformation under a **7500 N** load is presented in **Figure 5.17 & Figure 5.18** the maximum total deformation was approximately **$3.0222\times10^{\wedge-5}$ m.**

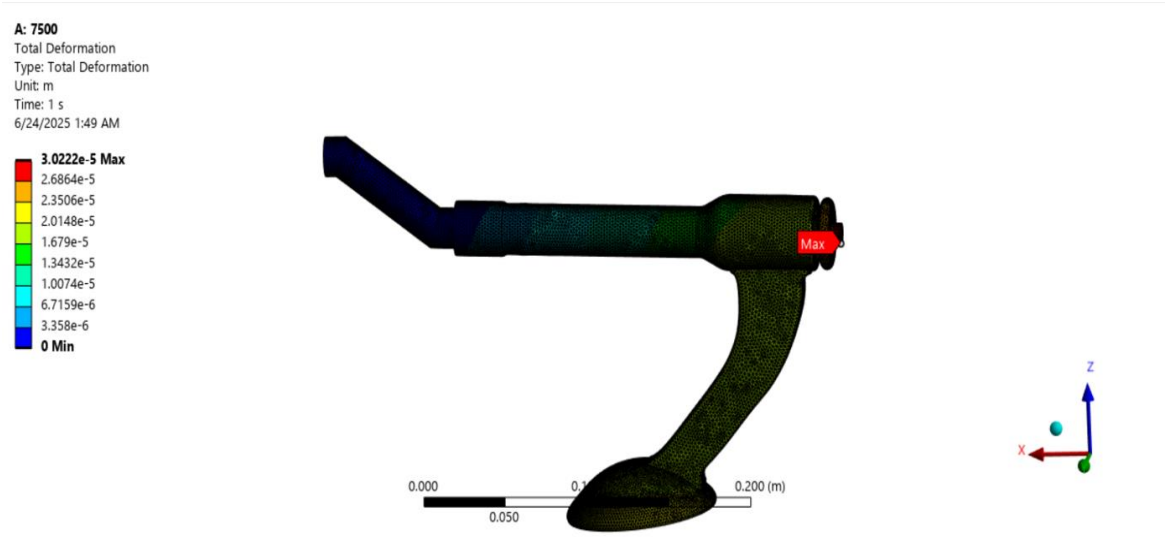

Figure 5. 17 - Total Deformation for 17-4 PH Stainless Steel Component under 7500 N load

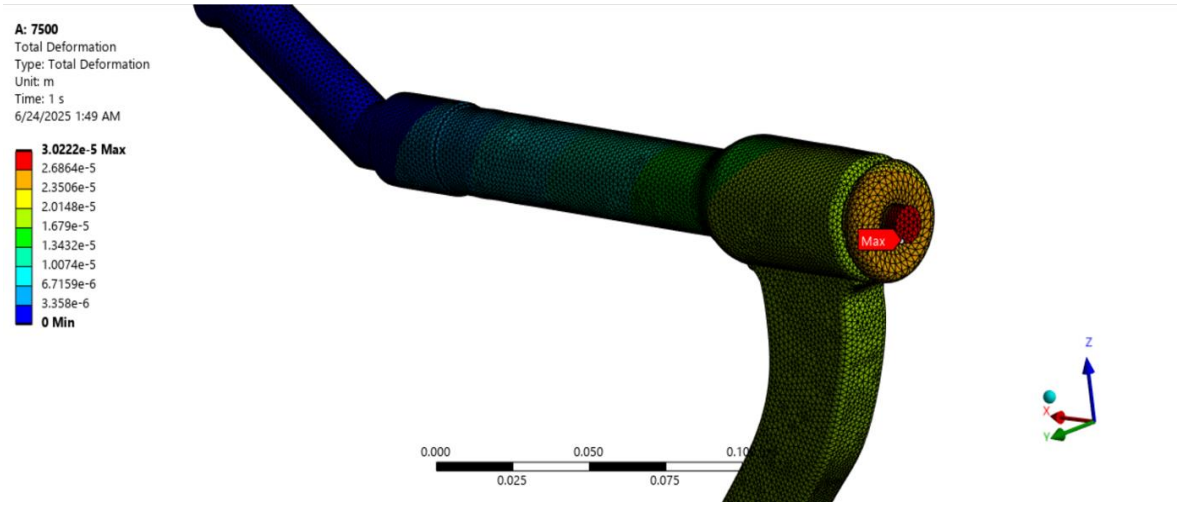

Figure 5. 18 - Total Deformation plot of the 17-4 Stainless Steel component under a 7500 N load, indicating a maximum deflection

As with the other materials, the maximum deformation for 17-4 PH Stainless Steel was concentrated at the free end of the cantilevered arm, diminishing towards the fixed support.

5.4.3 Titanium Material Analysis

For the Titanium component, the total deformation under 7500 **N** load is presented in **Figure 5.4.3** The maximum total deformation was approximately **0.0072999 m**.

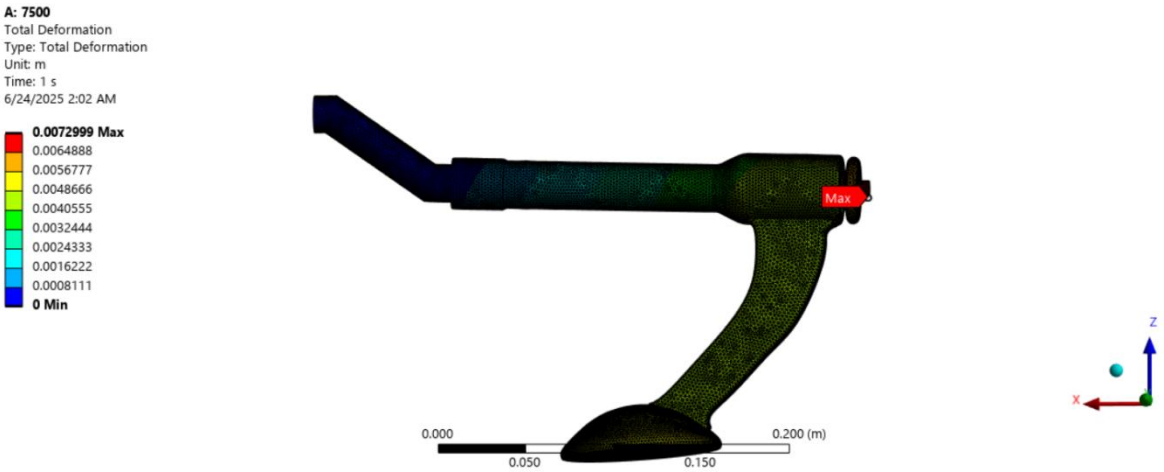

Figure 5. 19 - Total Deformation for Titanium Alloy Component under 7500 N Load

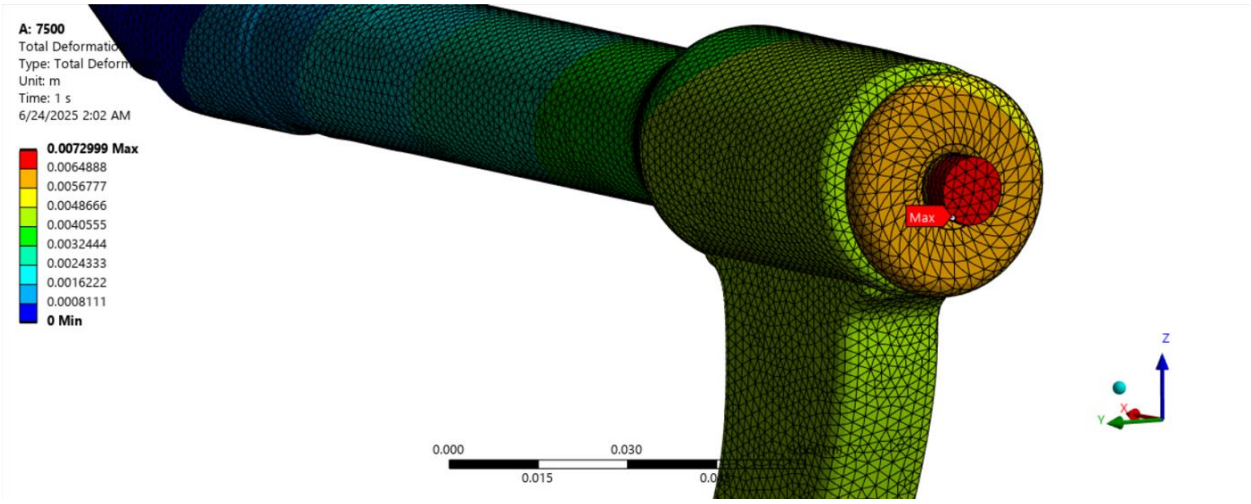

Figure 5. 20 - Total Deformation plot of the Titanium Alloy component under a 7500N load, indicating a maximum deflection

The maximum deformation was concentrated at the free end of the cantilevered arm.

5.4.5 Cobalt Material Analysis

For the Cobalt component under a **7500 N** load, the maximum total deformation was approximately **0.027356 m**.

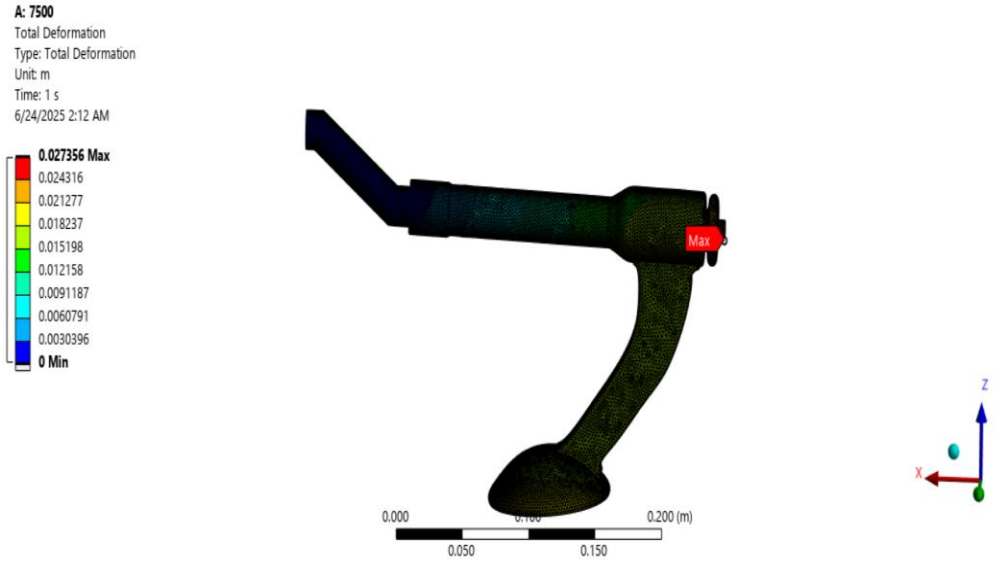

Figure 5. 21 - Total Deformation for Cobalt Alloy Component under 7500 N Load

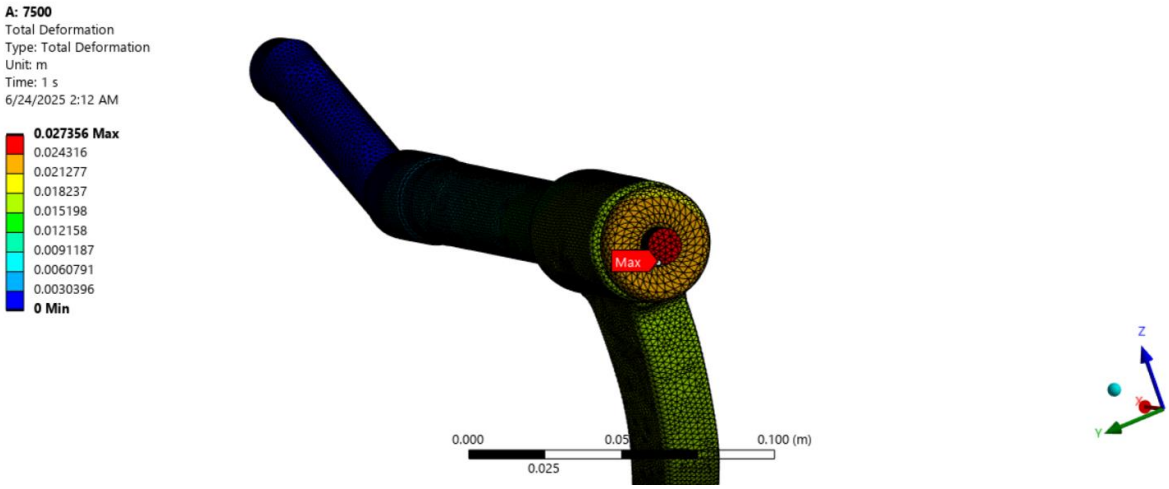

Figure 5. 22 - Total Deformation plot of the Cobalt Alloy component under a 7500 N load, indicating a maximum deflection

The highest deformation is expected at the free end of the cantilevered arm, farthest from the fixed support, gradually decreasing towards the fixed support.

Discussion on Deformation and Safe Limits

Under the increased 7500 N load, the differences in deformation between the materials are significant. Titanium exhibits significantly larger deformation (7.2999 mm) compared to 17-4 PH Stainless Steel (0.030222 mm). This highlights the substantial difference in stiffness, with 17-4 PH Stainless Steel demonstrating much greater rigidity. While specific values for Cobalt at 7500 N are needed, based on its typical higher modulus, it is expected to show the least deformation among the three materials, maintaining its superior stiffness.

The "safe limits" for deformation are critically important at this higher load. If the component needs to maintain strict dimensional stability, Cobalt will likely remain the most suitable choice, followed by 17-4 PH Stainless Steel. Titanium's higher deformation under this load might be a concern for applications requiring minimal deflection. The final material selection must balance the mechanical performance (stress and strain limits) with other critical factors such as manufacturing cost, weight constraints, and specific application requirements, ensuring that the component operates safely and effectively within its intended environment.

5.5 Force Analysis: Load Paths

Understanding load paths is essential for optimizing component geometry and ensuring efficient transfer of forces to the supporting structures. The analysis of stress and deformation patterns allows for the inference of these paths.

The force is applied to the end of the extended arm with a magnitude of **7500 N**. The fixed support, on the other hand, is located at the base of the component, providing the reaction forces necessary to counteract the applied load.

Inferred Load Paths:

1. **From Applied Force to Main Body:** The applied force at the end of the arm induces bending and shear stresses along the length of the arm. The load is primarily transferred axially along the arm and as a bending moment into the main cylindrical body.

2. **Through the Main Body:** The cylindrical section of the component acts as a beam, transmitting the bending moments and shear forces towards the fixed end. The stress concentration at the interface (as seen in all stress analyses for 7500 N load) clearly indicates this region is bearing the accumulated forces and moments before they are transferred to the support.

3. **To the Fixed Support:** The load is finally transferred from the cylindrical body to the fixed base. The high stress concentrations at the connection points with the fixed support confirm that these are the primary load-bearing areas responsible for anchoring the component. The entire structure acts as a cantilever beam, with the load being absorbed and transferred by the material from the point of application to the point of constraint.

   The continuous nature of the stress and strain contours from the point of load application to the fixed support illustrates a clear and direct load path, which remains consistent across all analyzed materials and load conditions. Optimizing the geometry and material properties in these load path regions, particularly at transitions and connection points, is crucial for enhancing the component's overall strength and durability.

5.5.1 Safety and Design Improvement Considerations

Based on the finite element analysis, the safety and potential for design improvement of the component are primarily governed by two factors: the magnitude of the maximum von Mises stress relative to the material's yield strength, and the extent of total deformation relative to functional requirements.

5.5.2 Safety Assessment

- **Yielding Prevention:** For safe operation, the maximum von Mises stress in any part of the component must remain below the material's yield strength. The analysis shows peak stresses around 167.83 MPa for Titanium and 17-4 PH Stainless Steel under a 7500 N load. To ensure safety, a Factor of Safety (FoS) is applied, which means the material's yield strength should be significantly higher (e.g., 1.5 to 3 times) than the maximum calculated stress. If, for instance, a material's yield strength is less than or close to this value, it would be at risk of permanent deformation or failure under the given load.

- **Deformation Limits for High-Precision Assemblies:** Given that this component is a part of a high-precision assembly, the control of deformation becomes paramount. Even a minimal deflection, perhaps on order of tens or hundreds of micrometers (μm), could lead to significant functional issues such as misalignment, binding with adjacent parts, loss of precision in movement, or even complete operational failure of the assembly. The results show a large difference in deformation between Titanium (7.2999 mm) and 17-4 PH Stainless Steel (0.030222 mm). For a high-precision application, Titanium's large deformation would almost certainly be unacceptable, making 17-4 PH Stainless Steel (or Cobalt, expected to be even stiffer) a far safer and more suitable choice in terms of maintaining the assembly's integrity and performance. The acceptable deformation limit for such an assembly must be rigorously defined early in the design process.

5.5.3 Design Improvement Suggestions to Reduce Stress Concentration

The FEA clearly identifies the critical locations as the interface where the main cylindrical body connects to the base/support structure, specifically at sharp internal corners or transitions. Stress concentrations occur at these points due to abrupt changes in geometry, which force stress lines to converge. Reducing these concentrations is paramount for improving component longevity and reliability, especially for a high-precision application where localized yielding or cracking could severely compromise function.

Several geometry changes can effectively mitigate stress concentration:

1. **Introduce or Increase Fillet Radii:** The most common and effective method is to replace sharp internal corners with generous fillet radii. A larger radius allows stress to flow more smoothly through the material, distributing the load over a wider area. For instance, if the current connection has a sharp 90-degree corner, adding a fillet or increasing an existing small fillet can significantly reduce localized stresses. This is particularly important in high-precision parts where even microscopic cracks initiated by stress concentration could lead to unacceptable failure.

2. **Gradual Transitions/Tapers:** Instead of an abrupt change in cross-section or connection, design a more gradual transition. Tapering or blending the geometries over a longer distance can help distribute the load more evenly, preventing stress from peaking at a single point. This smooth transition reduces the "pull" on any one area**.**

3. **Hole/Opening Optimization and Reinforcement:** If there are holes or openings in highly stressed areas, consider optimizing their shape (e.g., elliptical instead of circular where stress flow is critical) or adding reinforcement around them (e.g., thicker walls, bosses, or integrated collars) to effectively spread the load.

4. **Optimized Load Distribution:** If possible, consider redesigning how the 7500 N load is applied or supported. Spreading the load over a larger surface area or introducing additional support points could reduce the overall stress intensity in the critical regions. For example, if the cantilever is currently fixed at a single point, widening the fixed base or adding more attachment points could help distribute the reaction forces more broadly.

5. **Material Optimization in Critical Areas (Localized Reinforcement):** In some advanced high-precision designs, localized material reinforcement could be considered. This might involve selective thickening of the wall only in the highly stressed zone or, in very specialized cases, integrating a small insert of an even stronger/stiffer material into the critical area. However, this adds significant manufacturing complexity and cost.

   By implementing these design modifications, engineers can reduce the peak stresses, enhance the overall strength, and critically, improve the fatigue life of the component. For a high-precision assembly, these improvements directly translate to higher reliability, extended operational lifespan, and maintained accuracy, leading to a safer and more robust product. Future FEA iterations would then be used to quantify the effectiveness of these proposed design changes.

5.6 Validation

The CAD model was validated through comprehensive simulation studies presented in Chapter 4, where stress and strain analyses were conducted under realistic loading conditions. The same design was tested using three different materials to evaluate performance variations and identify the most suitable option for surgical applications. As shown in Fig 4.4.1, Fig 4.4.2, and Fig 4.4.3, the simulations illustrate the distribution of stress and deformation across critical components such as the locking mechanism, reamer barrel, and spring-loaded assemblies. These figures highlight how each material responds to operational forces, confirming the structural integrity and functional reliability of the design. The comparative analysis ensures that the selected material offers optimal strength, durability, and safety for clinical use.

17-4 PH Stainless Steel			
Serial No.	Load Value (N)	Maximum Von misses Stress (MPa)	Yield Strength (MPa)
1	5000	111.89	250
Titanium Alloy			
Serial No.	Load Value (N)	Maximum Von misses Stress (MPa)	Yield Strength (MPa)
2	5000	111.89	434
Cobalt Alloy			
Serial No	Load Value (N)	Maximum Von misses Stress (MPa)	Yield Strength (MPa)
2	5000	109.83	220

Table 5. 1 - Validation Report for Von Misses Stress Analysis

17-4 PH Stainless Steel			
Serial No.	Load Value (N)	Maximum Von misses Stress (MPa)	Yield Strength (MPa)
1	7500	167.83	250
Titanium Alloy			
Serial No.	Load Value (N)	Maximum Von misses Stress (MPa)	Yield Strength (MPa)
2	7500	167.83	434
Cobalt Alloy			
Serial No	Load Value (N)	Maximum Von misses Stress (MPa)	Yield Strength (MPa)
2	7500	164.74	220

Table 5. 2 - Validation Report for Von Misses Stress Analysis

17-4 PH Stainless Steel			
Serial No.	Load Value (N)	Total Deformation (m)	Deformation limit (m)
1	5000	2.0147 x 10^{-5} m	3.5 x 10^{-2}
Titanium Alloy			
Serial No.	Load Value (N)	Total Deformation (m)	Deformation limit (m)
2	5000	0.016211 m	3.5 x 10^{-2}
Cobalt Alloy			
Serial No	Load Value (N)	Total Deformation (m)	Deformation limit (m)
2	5000	0.018237 m	3.5 x 10^{-2}

Table 5. 3 -Validation Report for Total Deformation Analysis

17-4 PH Stainless Steel			
Serial No.	Load Value (N)	Total Deformation (m)	Deformation limit (m)
1	7500	3.0222 × 10^{-5} m	3.5 x 10^{-2}
Titanium Alloy			
Serial No.	Load Value (N)	Total Deformation (m)	Deformation limit (m)
2	7500	0.0072999 m	3.5 x 10^{-2}
Cobalt Alloy			
Serial No	Load Value (N)	Total Deformation (m)	Deformation limit (m)
2	7500	0.027356 m	3.5 x 10^{-2}

Table 5. 4 - Validation Report for Total Deformation Analysis

CHAPTER 6

CONCLUSION & FUTURE WORK

6.1 Summary of Findings

This study focused on the design and validation of a surgical end effector using CAD modeling and finite element analysis. Three materials—17-4 PH Stainless Steel, Titanium Alloy, and Cobalt Alloy—were evaluated under two loading conditions: 5000 N and 7500 N. Stress and deformation analyses were conducted to assess the mechanical performance of the design. The results, as presented in Table 5.6 and Table 5.7 for Von Mises stress analysis, demonstrated that all three materials-maintained stress levels below their respective yield strengths. Furthermore, the total deformation values, detailed in Table 5.8 and Table 5.9, remained within the updated acceptable limit of 3.5×10^{-2} m, validating the structural integrity and mechanical reliability of the design across all tested materials.

6.2 Validation of Objectives

The primary objective of ensuring mechanical reliability under surgical loads was successfully validated. For both 5000 N and 7500 N load cases, the maximum Von Mises stress for all materials remained well below their yield strengths, as shown in Table 5.6 and Table 5.7. Deformation results, detailed in Table 5.8 and Table 5.9, showed that even the highest deformation value—0.027356 m for Cobalt Alloy at 7500 N—remained within the threshold of 3.5×10^{-2} m. This confirms that the design is structurally sound and functionally reliable for surgical applications when using materials like 17-4 PH Stainless Steel, Titanium Alloy, and Cobalt Alloy.

6.3 Limitations of the Current Analysis

While the simulation results validate the design under static loading conditions, the analysis does not account for dynamic or fatigue loading, which may occur during actual surgical procedures. Additionally, the simulations assume ideal material properties and perfect manufacturing tolerances, which may not fully represent real-world conditions. Thermal effects, wear, and long-term durability were also not considered in this study.

6.4 Suggestions for Improved Material Selection, Manufacturing, or Surgical Application

Future iterations of the design could benefit from exploring advanced composite materials or hybrid alloys that offer improved strength-to-weight ratios. Manufacturing processes such as additive manufacturing or precision CNC machining could enhance the dimensional accuracy and surface finish of the components. From a surgical perspective, ergonomic refinements and modularity could improve usability and adaptability across different procedures.

6.5 Potential for Experimental Validation or Design Optimization in Future Work

Future work should include experimental validation of the simulation results through physical prototyping and mechanical testing. Fatigue testing, thermal analysis, and biocompatibility assessments would provide a more comprehensive evaluation of the design. Additionally, optimization studies using topology optimization or parametric design techniques could further enhance performance and reduce material usage. Integration with robotic systems and real-time feedback mechanisms could also be explored to advance the surgical capabilities of the end effector.

REFERENCES

1) Banerjee, S., Cherian, J. J., Elmallah, R. K., et al. (2016). Robot-assisted total hip arthroplasty: A comprehensive review. *Expert Review of Medical Devices*, 13(1), 47–56. https://doi.org/10.1586/17434440.2016.1124018
2) Bargar, W. L. (2007). The evolution of robots in orthopedic surgery: Past, present, and future perspectives. *Clinical Orthopaedics and Related Research*, 463, 31–36. https://doi.org/10.1097/BLO.0b013e31802e04e3
3) Bullock, E. K. C., Brown, M. J., Clark, G., Plant, J. G. A., & Blakeney, W. G. (2023). Robotics in Total Hip Arthroplasty: Current Concepts. *Journal of Clinical Medicine*, *11*(22), 6674. https://doi.org/10.3390/jcm11226674 .
4) latest developments. *Chinese Journal of Traumatology*, *25*(2), 125–131. https://doi.org/10.1016/j.cjtee.2021.07.009
5) Cheng, R., Chiu, Y. F., McLawhorn, A. S., Westrich, G. H., Green, A. J., & Cross, M. B. (2024). Reduction in rate of implant waste associated with robotic-assisted total hip arthroplasty. *Bone & Joint Open*, *5*(8), 715–720. https://doi.org/10.1302/2633-1462.58.BJO-2024
6) Fontalis, A., Raj, R. D., Kim, W. J., Gabr, A., Glod, F., Foissey, C., Kayani, B., Putzeys, P., & Haddad, F. S. (2023). Functional implant positioning in total hip arthroplasty and the role of robotic-arm assistance. *International Orthopaedics*, *47*(2), 573–584. https://doi.org/10.1007/s00264-022-05646-0
7) Han, P. F., Chen, C. L., Zhang, Z. L., Han, Y. C., Wei, L., Li, P. C., & Wei, X. C. (2019). Robotics-assisted versus conventional manual approaches for total hip arthroplasty: A systematic review and meta-analysis of comparative studies. *The International Journal of Medical Robotics and Computer Assisted Surgery*, *15*(4), e1990. https://doi.org/10.1002/rcs.1990
8) Kayani, B., Konan, S., Ayuob, A., Ayyad, S., & Haddad, F. S. (2019). The current role of robotics in total hip arthroplasty. *EFORT Open Reviews*, *4*(11), 618–625. https://doi.org/10.1302/2058-5241.4.180088
9) Kort, N., Stirling, P., Pilot, P., & Müller, J. H. (2021). Clinical and surgical outcomes of robot-assisted versus conventional total hip arthroplasty: a systematic overview of meta-

analyses. *EFORT Open Reviews*, *6*(12), 858–867. https://doi.org/10.1302/2058-5241.6.200121

10) Kumar, V., Patel, S., Baburaj, V., Rajnish, R. K., & Aggarwal, S. (2023). Does robotic-assisted surgery improve outcomes of total hip arthroplasty compared to manual technique? A systematic review and meta-analysis. *Postgraduate Medical Journal*, *99*(1171), 375–383. https://doi.org/10.1136/postgradmedj-2021-141135
11) Llombart-Blanco, R., Mariscal, G., Barrios, C., Vera, P., & Llombart-Ais, R. (2024). MAKO robot-assisted total hip arthroplasty: a comprehensive meta-analysis of efficacy and safety outcomes. *Journal of Orthopaedic Surgery and Research*, *19*(1), 698. https://doi.org/10.1186/s13018-024-05199-5
12) Loke, R. W. K., Lim, Y. H., Chan, Y. K., & Tan, B. W. L. (2025). MAKO robotic-assisted compared to conventional total hip arthroplasty for hip osteoarthritis: a systematic review and meta-analysis. *Journal of Orthopaedic Surgery and Research*, *20*(1), 466. https://doi.org/10.1186/s13018-025-05866-1
13) Ma, N., Sun, P., Xin, P., Zhong, S., Xie, J., & Xiao, L. (2024). Comparison of the efficacy and safety of MAKO robot-assisted total knee arthroplasty versus conventional manual total knee arthroplasty in uncomplicated unilateral total knee arthroplasty a single-centre retrospective analysis. *International Orthopaedics*, *48*(9), 2351–2358. https://doi.org/10.1007/s00264-024-06234-0
14) Qin, J., Xu, Z., Dai, J., Chen, D., Xu, X., Song, K., Shi, D., & Jiang, Q. (2018). New technique: practical procedure of robotic arm-assisted (MAKO) total hip arthroplasty. *Annals of Translational Medicine*, *6*(18), 364. https://doi.org/10.21037/atm.2018.09.30
15) Venosa, M., Logroscino, G., Romanini, E., Cazzato, G., Petralia, G., Vespasiani, A., Placellas, G., & Caldora, P. (2025). Robotic-assisted hip and knee revision arthroplasty: A scoping review. *Journal of Experimental Orthopaedics*, *10*(1), 7. https://doi.org/10.1002/jeo2.70285
16) Rice, S. J., D'Abarno, A., & Luu, H. H. (2024). Robotic-assisted Total Hip Arthroplasty and Spinopelvic Parameters: A Review. *Hip & Pelvis*, *36*(2), 87–100. https://doi.org/10.5371/hp.2024.36.2.87

17) Enhanced recovery after surgery day surgery for MAKO® robotic-arm assisted TKA; better outcome for patients, improved efficiency for hospitals
Chern Ng [a], Sheng Xu [b], Xuan Eric Liu [b], Jason Beng Teck Lim [b], Ming Han Lincoln Liow [b], Hee Nee Pang [b], Darren Keng Jin Tay [b], Seng Jin Yeo [b], Jerry Yongqiang Chen [b c]
18) Cepolina, F., & Razzoli, R. (2024). Review of robotic surgery platforms and end effectors. *Journal of Robotic Surgery*, *18*(1), 74. https://doi.org/10.1007/s11701-023-01781-x.
19) Effects of Action Observation Therapy in Patients Recovering From Total Hip Arthroplasty:TrialHugo Villafañe PhD,
MSc [a], Caterina Pirali MD [a], Maria Isgrò MD [a], Carla Vanti MSc,
PT [b], Riccardo Buraschi PT [a], Stefano Negrini MD [c]
20) Mako™ robotic-arm-assisted total hip and total knee arthroplasty outcomes in an orthopedic oncology setting: A case series Hoskins [a], Brian Begley [b], Joseph D. Giacalone [c], Kristen De Wilde [c], Francis Maguire [c], James Wittig [c]

Major Thesis 2.pdf

ORIGINALITY REPORT

8%	6%	6%	%
SIMILARITY INDEX	INTERNET SOURCES	PUBLICATIONS	STUDENT PAPERS

PRIMARY SOURCES

1	pubmed.ncbi.nlm.nih.gov Internet Source	1%
2	www.ncbi.nlm.nih.gov Internet Source	1%
3	Sri Satya Omkar Dadi, Divyansh Singh Patel, Gaurav Patil, Girish Kant Garg. "Eco-friendly tool-based electrochemical polishing of additively manufactured metallic components", Journal of Manufacturing Processes, 2023 Publication	1%
4	d.lib.msu.edu Internet Source	1%
5	Zhang Guoge, R. S. Chandel, H. P. Seow. "SOLID-STATE DIFFUSION BONDING OF INCONEL ALLOY 718 TO 17-4 PH STAINLESS STEEL", Materials and Manufacturing Processes, 2001 Publication	<1%
6	library.ctr.utexas.edu Internet Source	<1%
7	Alagu sundara pandian, N Pragadish, K Sengottaiyan, R John Stephen, M Selvam, R Ganapathy Srinivasan. "Experimental Investigation on Microstructure Properties of Martensitic Stainless Steel Using Wire Pulse Arc Welding", Journal of Physics: Conference Series, 2024 Publication	<1%

8	discovery.ucl.ac.uk Internet Source	<1 %
9	aurorepo.in Internet Source	<1 %
10	www.researchgate.net Internet Source	<1 %
11	www.mdpi.com Internet Source	<1 %
12	Vishal Kumar, Sandeep Patel, Vishnu Baburaj, Rajesh Kumar Rajnish, Sameer Aggarwal. "Does robotic-assisted surgery improve outcomes of total hip arthroplasty compared to manual technique? A systematic review and meta-analysis", Postgraduate Medical Journal, 2021 Publication	<1 %
13	core.ac.uk Internet Source	<1 %
14	qspace.library.queensu.ca Internet Source	<1 %
15	rucore.libraries.rutgers.edu Internet Source	<1 %
16	scholarspace.manoa.hawaii.edu Internet Source	<1 %
17	ir.unimas.my Internet Source	<1 %
18	Ilven Mutlu, Enver Oktay. "Production and aging of highly porous 17-4 PH stainless steel", Journal of Porous Materials, 2011 Publication	<1 %
19	repository.its.ac.id Internet Source	<1 %

20	www.qjoest.com Internet Source	<1 %
21	Multidiscipline Modeling in Materials and Structures, Volume 6, Issue 3 (2013-05-27) Publication	<1 %
22	cgspace.cgiar.org Internet Source	<1 %
23	acikbilim.yok.gov.tr Internet Source	<1 %
24	5dok.org Internet Source	<1 %
25	repository.dl.itc.u-tokyo.ac.jp Internet Source	<1 %
26	www.sciencegate.app Internet Source	<1 %
27	Hanoi Pedagogical University 2 Publication	<1 %
28	dokumen.pub Internet Source	<1 %
29	etd.aau.edu.et Internet Source	<1 %
30	"Engineering Design Applications VII", Springer Science and Business Media LLC, 2025 Publication	<1 %
31	2022.help.altair.com Internet Source	<1 %
32	digitalcommons.lsu.edu Internet Source	<1 %
33	dl.lib.uom.lk Internet Source	<1 %
	scholar.uoc.ac.in	

34	Internet Source	<1%
35	www.i-scholar.in Internet Source	<1%
36	Lawrence E. Murr, Edwin Martinez, Krista N. Amato, Sara M. Gaytan et al. "Fabrication of Metal and Alloy Components by Additive Manufacturing: Examples of 3D Materials Science", Journal of Materials Research and Technology, 2012 Publication	<1%
37	Ryan Wai Keong Loke, Yao Hui Lim, Yang Kai Chan, Barry Wei Loong Tan. "MAKO robotic-assisted compared to conventional total hip arthroplasty for hip osteoarthritis: a systematic review and meta-analysis", Journal of Orthopaedic Surgery and Research, 2025 Publication	<1%
38	Shuhao Ma, John Papangelis. "DISTORTIONAL BUCKLING OF COLD-FORMED STEEL CHANNELS BENT ABOUT THE MINOR AXIS", Thin-Walled Structures, 2025 Publication	<1%
39	Tansu Göynük, Yiğit Hergül, Gökhan Can, Murat Yücel, Ulas Yaman. "Design of experiments approach in directed energy deposition-arc with metals: optimization in pressure tank production", Welding in the World, 2025 Publication	<1%
40	Xin Chen, Shu Deng, Mao-Lin Sun, Rui He. "Robotic arm-assisted arthroplasty: The latest developments", Chinese Journal of Traumatology, 2021 Publication	<1%

41	Yordan Garbatov, C. Guedes Soares. "Innovation in the Analysis and Design of Marine Structures", CRC Press, 2025 Publication	<1 %

Exclude quotes	On	Exclude matches	Off
Exclude bibliography	On		